Section 1

Atmospheric data assimilation schemes, analysis and initialization, data impact studies, observing system experiments

Impact of realistic soil moisture initialization on 1-month forecast of continental precipitation.

Marie Boisserie (marie@coaps.fsu.edu), Steve Cocke, D. W. Shin and Jim O'Brien, COAPS/FSU, Tallahassee, FL, USA.

Although the amount of water contained in the soil seems insignificant when compared to the total amount of water on a global-scale, soil moisture is widely recognized as a crucial variable for climate studies. It plays a key role in regulating the interaction between the atmosphere and the land-surface by controlling the repartition between the surface latent and sensible heat fluxes. In addition, the persistence of soil moisture anomalies provides one of the most important components of memory for the climate system. Several studies have shown that, during the boreal summer in mid-latitudes, the soil moisture role in controlling the continental precipitation variability may be more important than that of the sea surface temperature (Hong and Kalnay 2000, Koster et al. 2000, Kumar and Hoerling 1995, Trenberth et al. 1998, Shukla 1998).

Although all of the above studies have demonstrated the strong sensitivity of seasonal forecasts to the soil moisture initial conditions, they have relied on extreme or idealized soil moisture levels. The question of whether realistic soil moisture initial conditions lead to improved seasonal predictions has not been adequately addressed. Progress in addressing this question has been hampered by the lack of long-term reliable observation-based global soil moisture data sets. Since precipitation strongly affects the soil moisture characteristics at the surface and in depth, an alternative to this issue is to assimilate precipitation. Because precipitation is a diagnostic variable, most of the current reanalyses do not directly assimilate it into their models (M. Bosilovitch, 2008). In this study, an effective technique that directly assimilates the precipitation is used.

We examine two experiments. In the first experiment (here after, series 1), the land-atmosphere Florida State University/Center for Ocean and Atmosphere Predictions Studies (FSU/COAPS) model is initialized by directly assimilating a global, 3-hourly, 1.0° precipitation dataset, provided by Sheffield et al. (2006), in a continuous assimilation period of a couple of months. For this, we use a technique named the Precipitation Assimilation Reanalysis (PAR) and described in Nunes and Cocke (2004). This technique consists of modifying the vertical profile of humidity as a function of the observed and predicted model rain rates. In the second experiment, the model is initialized without precipitation assimilation. For each series, 50 sets of 1-month forecast are generated. The forecast starting dates are the 1st of each month between April and August and each year between 1986 and 1995. Since, series 1 and series 2 differs only from the initialization method of the land surface state, by taking the difference between series 1 and series 2, it will show the effect of the realistic soil moisture initialization on the forecasting skills of the model.

The Figure 1 shows the correlation squared of raw precipitation and anomaly precipitation between each series and the observation. The precipitation observation used here, is the daily precipitation reanalysis of Higgins et al. (2000). For both the raw precipitation and the anomaly, the series-1 skills are significantly larger than the series-2 skills in the northern U.S with an increase skill up to 24%. On average across U.S, the 1-month forecast skills are increased by 1.2%. These results indicate that, this soil moisture initialization technique has the potential to increase the 1-month forecast skills of precipitation in the northern U.S.

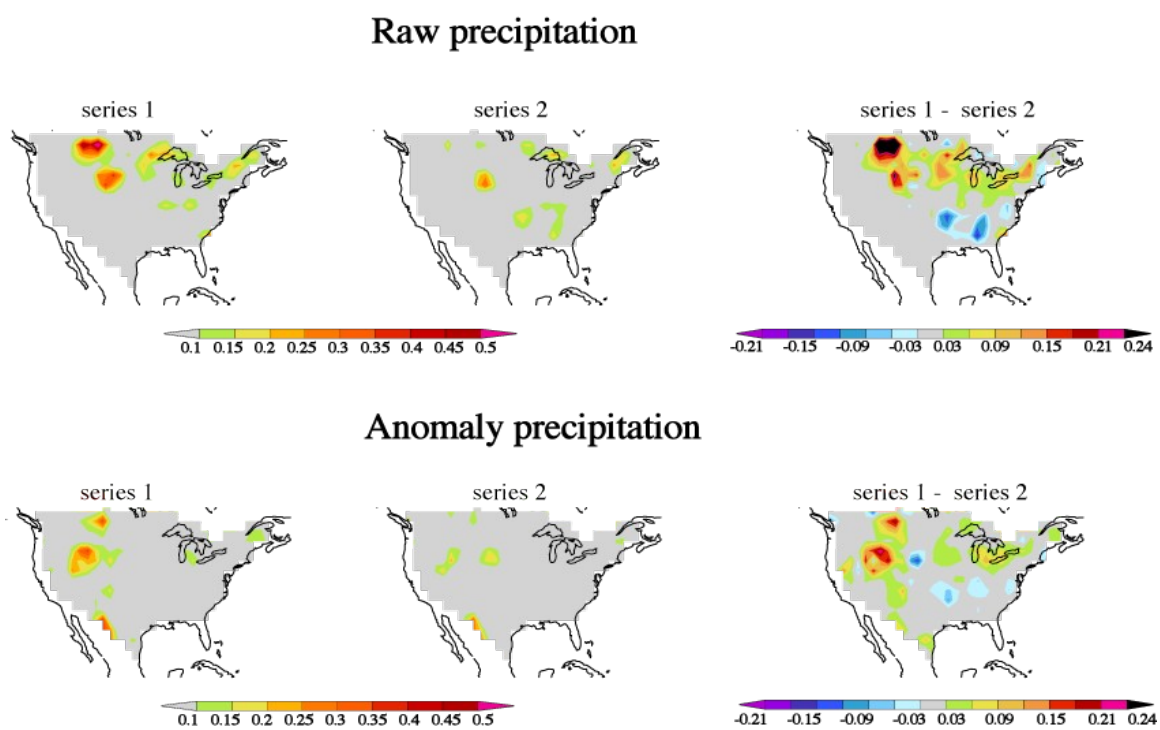

Figure 1: Spatial distribution of correlations squared (r^2) between FSU/COAPS model and the precipitation observation of the raw data (top) and the anomaly (bottom), for the series 1 (left), series 2 (middle) and the difference (right).

Using HDO and H_2O Measurements from the Tropospheric Emission Spectrometer to Constrain a Quasi-Lagrangian Mass Transport Model

Derek Brown and David Noone
Cooperative Institute for Research in Environmental Sciences (CIRES)
University of Colorado at Boulder, CO, USA (email: derek.brown@colorado.edu)

Stable water isotopes are useful in diagnosing the global hydrologic cycle since isotopic fractionations, which occur during evaporation and condensation, give rise to measurable variations in the isotopic composition of water vapor. In this study, a quasi-Lagrangian mass transport model assumes that the balances of moisture and isotopes along trajectories arriving at Tropospheric Emission Spectrometer (TES) observation sites are explained by losses from precipitation and gains via turbulent transport from the near-surface.

Vertically integrated H_2O (hereafter *q*) and HDO/H_2O (hereafter *R*) values are found at the TES observation locations using the mass weighted values from the respective TES profiles for the 500-825 hPa layer. In order to establish a Lagrangrian framework with which to study the regional isotopic budgets, back trajectories originating from each TES observation location from September, 2004 to March, 2008 (614064 instantaneous observations) were calculated, assuming an arrival height in the middle of the 500-825 hPa layer.

Along the set of back trajectories, the TES observations that occur within one hour and one half of a degree along the one to three day portions of the back trajectories are found (hereafter crossings). Derived values of *q* and *R* at the crossings are found from the respective TES profiles using the vertically integrated, mass weighted values for the 325 hPa thick layer centered at the pressure level of the parcel (as deduced from the trajectory model). As such, the net result is 95963 one to three day back trajectories with endpoints in three dimensional space containing mass weighted TES *q* and *R* values found over a 325 hPa thick layer.

Using these segments, we have devised a model with two budget equations that approximates the gains and losses of water and deuterium into and out of the parcels. The equation for change in water amount over time along the trajectories is represented simply as

$$\frac{\partial q}{\partial t} = S - L = k(q_s - q) - aq \qquad (1)$$

where the terms, *S* and *L* [(mm of H_2O)]/day], represent the rate of supply of water by turbulent transport and the loss of water via precipitation, respectively. The rate parameters *k* and *a* (days^{-1}) are used as free variables to solve for the timescales of refreshment and losses of moisture into and from the parcels, respectively. The term, q_s (mm of H_2O), represents the saturation specific humidity at the moisture source region, and is a function of near-surface temperature. A similar budget for deuterium (hereafter *s,* which is equivalent to *Rq*) is represented by

$$\frac{\partial s}{\partial t} = S_s - L_s = k\mu(s_s - s) - a\alpha s \qquad (2)$$

where the terms, S_s and L_s [(mm of HDO)]/day], represent the rate of supply of HDO from turbulent transport and the loss of water via precipitation, respectively. Additionally, s_s is a free parameter representing the amount of HDO at the source region, μ represents kinetic isotopic fractionation during diffusive mixing (0.995 for this study), and α is a free parameter representing the effective isotopic fractionation during condensation.

Equations (1) and (2) may be integrated analytically to generate modeled values of q and R given the upwind q and R values, the length of the trajectories, and the free parameters in the model (k, a, s_s, and α). Minimization of the mass weighted, percent differences of modeled versus observed downstream values of q and R over a set of seasonal trajectories proceeds by use of a cost function,

$$J = \frac{\sum_{obs} \Theta^2 \cdot \left\{ \left[\frac{(q_{\text{mod}} - q_{obs})}{q_{obs}} \right]^2 + \left[\frac{R_{\text{mod}} - R_{obs}}{R_{obs}} \right]^2 \right\}}{\sum_{obs} \Theta^2}$$

where the term, Θ, represents mass weighting and is equal to q at the downstream TES observation. We use numerous trajectories ($n \geq 100$) to estimate the free parameters for the group as a whole that minimize the cost function, J, given that each trajectory in the group varies in length and has unique q and R values provided by TES. For five by five degree grid boxes over the domain 0-360E and 60S-60N, the set of trajectories used for each grid point is found by incorporating all trajectories that have their downstream TES observation within a circle of radius 1000 km (approximately ten degrees) from the location of the respective grid point. This method thus oversamples the trajectory information to produce a five by five degree grid of the best-fit parameters for each grid point.

Preliminary results show good agreement between moisture divergence values derived from our model (simply $S - L$) and those derived diagnostically from the NCEP/NCAR analysis (not shown). However, one advantage of the isotopic model is that we can separate out the source and loss components individually. **Figure 1** shows the timescale for moisture refreshment due to turbulent transport of near-surface moisture. The tropical convection zones show quick refreshment of moisture in the 500-825hPa layer, whereas the subtropical high-pressure areas show much longer timescales for moisture refreshment.

Figure 2 shows the effective equilibrium fractionation seen in the model runs. Fractionation over the monsoonal regions (SE Asian in JJA and N Australia and the Amazon in DJF) is greatest, as expected by 'amount effect' theory.

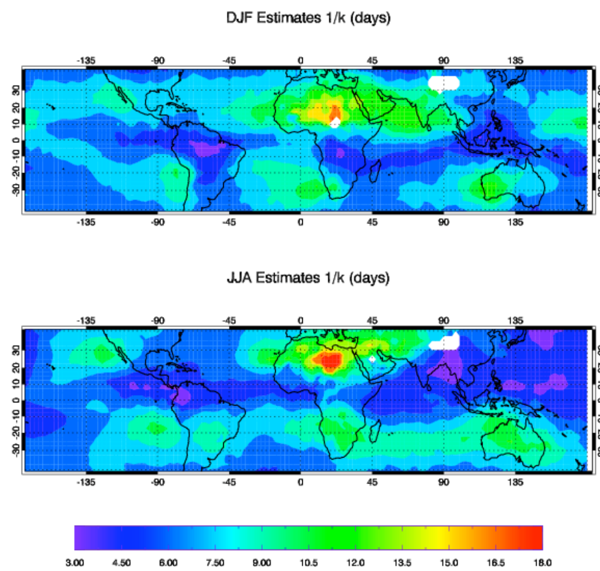

Figure 1: Timescale for H_2O refreshment in parcels

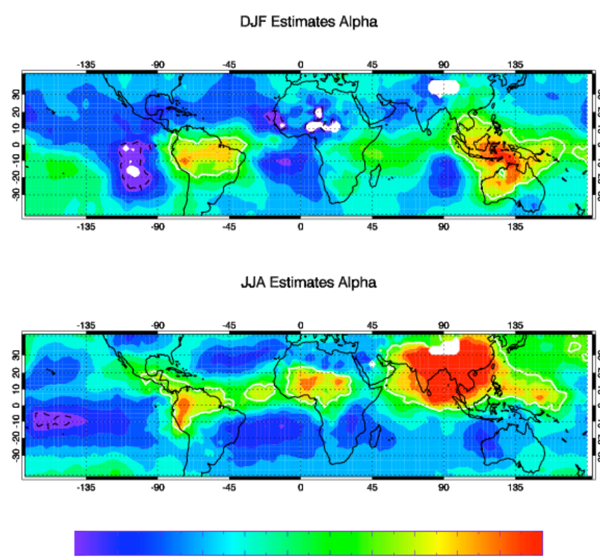

Figure 2: Effective equilibrium fractionation in parcels

Recent Updates of the JMA Hourly Analysis

Tadashi Fujita
Numerical Prediction Division, Japan Meteorological Agency
1-3-4 Otemachi, Chiyoda-ku, Tokyo 100-8122, Japan
(E-mail: t-fujita@met.kishou.go.jp)

1. Introduction

The JMA hourly analysis provides an hourly picture of three-dimensional temperature and wind distribution to assist forecasters in monitoring the atmosphere. A 3D-Var analysis is performed on a domain covering Japan and its surrounding area (about 3,600 km x 2,880 km) at a resolution of 5 km using the latest forecast from the operational mesoscale model (MSM) as the first guess. The observations assimilated in the analysis are from wind profilers (wind), Doppler radars (radial velocity), ACARS (Aircraft Communications Addressing and Reporting System, wind and temperature), satellite AMV (Atmospheric Motion Vector, wind), and AMeDAS (Automated Meteorological Data Acquisition System, surface station data over Japan, wind and temperature). The data cut-off time is set at 20 minutes past the hour to enable distribution of the product before 30 minutes past the hour.

2. Surface filter

A surface filter has recently been introduced to remedy the excessive analysis increment often found over the sea near the coastline. This unreasonably large increment is due to the assimilation of densely distributed surface observations on land (data from AMeDAS). In order to obtain a good fit to the surface observations on land, the 3D-Var analysis uses a short background error correlation distance and a small observation error on the surface. Thus, the surface field on land typically has a large increment. However, this

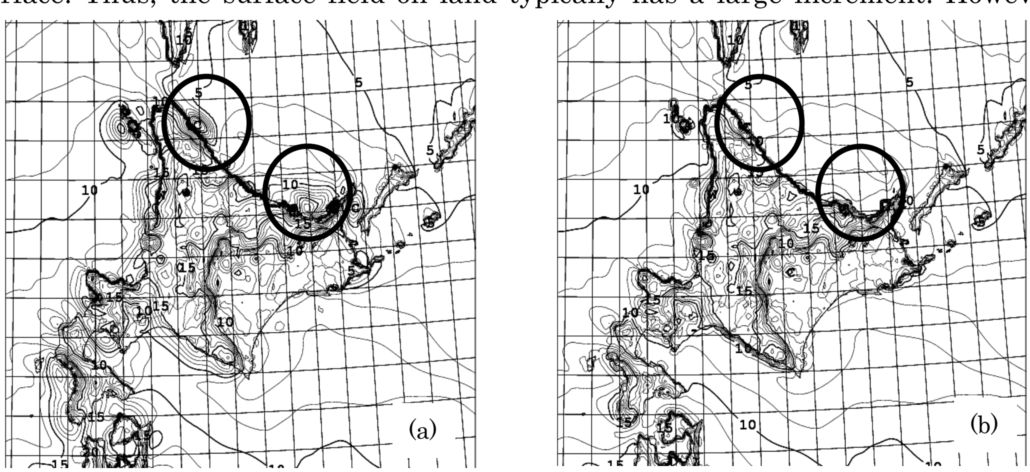

Fig. 1. Surface temperature from hourly analysis for 00 UTC on 19 May 2008 (degrees centigrade). (a) before applying the surface filter, (b) after applying the surface filter. Regions with an unreasonably large increment are marked with circles.

causes the problem of excessive increment in sea regions near the coastline located within the range of correlation from the land observations. Since no sea surface observation is currently used in the hourly analysis, the quality of the analysis in these regions is not necessarily high.

The surface filter is designed to attenuate the surface increment over the sea with distance from the coastline. This filter is applied to temperature and wind fields after the 3D-Var analysis. Figure 1 displays an example of surface temperature analysis before (Fig. 1 (a)) and after (Fig. 1 (b)) the surface filter is applied. It is found that the surface filter appropriately reduces the unreasonably large increment over the sea near the coastline (the circled parts).

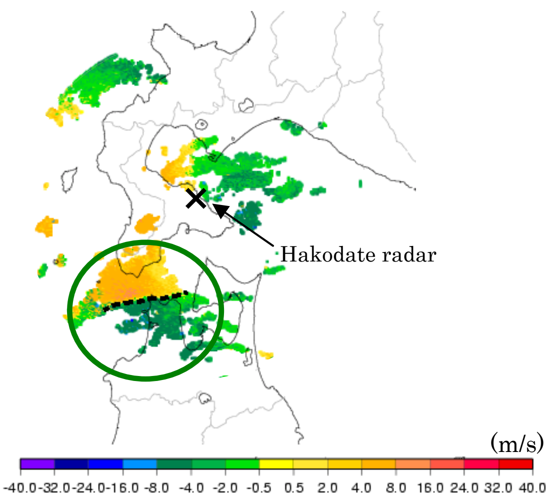

Fig. 2. Distribution of Doppler velocity at 03 UTC on 14 July 2008 from the Hakodate Doppler radar (elevation angle 0.4 deg.). 'x' indicates the location of the radar site. Cold colors show wind toward the site, and warm ones show wind away from it. The dashed curve shows the location of the wind shear line.

3. Radial velocity data from additional Doppler radar sites

In addition to radial velocity data from 12 JMA Doppler radar sites (including 8 airport sites) so far used in the hourly analysis, new radial velocity data from 7 more sites have been introduced. Figures 2 (observation) and 3 (analysis) show an example of the effect of the new data. Comparing the 850 hPa wind analysis fields obtained with (Fig. 3 (b)) and without (Fig. 3 (a)) radial velocity data from one of the additional sites (Hakodate), it is found that the new data help the analysis to better capture the location of the wind shear line (the black dashed curve).

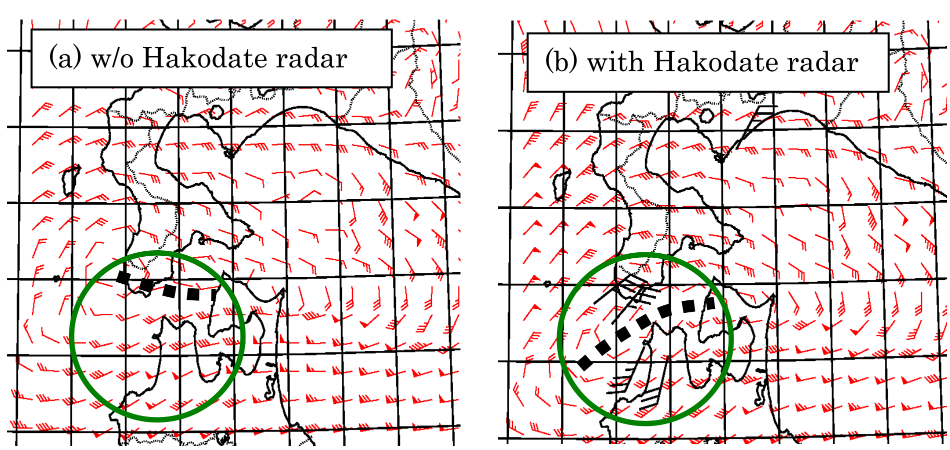

Fig. 3. 850 hPa wind from the hourly analysis for 03 UTC on 14 July 2008. (a) analysis without the Hakodate radar, (b) analysis with the Hakodate radar. Each half-flag of the wind barbs represents 1 m/s, full flag 2 m/s, pennant 10 m/s. The black wind barbs in (b) show the radial velocity used in the analysis. The dashed curves show the location of the wind shear line.

Spatial satellite observation-error statistics for AMSU-A data

Vadim Gorin and Mikhail Tsyrulnikov
Hydrometeorological Center of Russia
E-mails: vadicgor@gmail.com, tsyrulnikov@mecom.ru

1 Motivation

In the past, meteorological observations were scarce and inaccurate (as compared to the background). All we needed to know to optimally interpolate the observational information to grid points was observation-error *variances* and background-error *covariances*. Now, the situation is different. Satellite observations are comparable with the background both in accuracy and numbers. In addition, satellite observations, like the background, have spatially correlated errors due to state-dependent imperfections in their observation operators. As a result, poorly known and largely disregarded spatial statistics for satellite data seems to be now of comparable importance for data assimilation as the widely used background-error statistics.

The aim of this study is to objectively estimate the satellite observation-error spatial statistics for microwave AMSU-A observations known to be one of the most influential sources of observational information for numerical weather prediction.

2 Methodology

We compare bias-corrected satellite observations X_{sat}^{obs} with collocated radiosonde data X_{sond}^{obs} computing the differences $d = X_{sat}^{obs} - \mathcal{H}(X_{sond}^{obs})$, where $\mathcal{H}$ is the satellite observation operator. Our satellite bias-correction scheme ensures that d is unbiased. Averaging $d_i \cdot d_j$, where $i \neq j$ are indices of collocated pairs, we compute estimates of horizontal and inter-channel covariances for d. Our basic assumption is that errors of different radiosonde profiles are uncorrelated, which implies that covariances of d coincide with satellite-error covariances we seek to estimate.

Raw estimates of spatial covariances are smoothed with a moving-average filter and approximated by a truncated Fourier-Legendre series with non-negative coefficients (which yields positive definitness).

To estimate the 'white' (spatially uncorrelated) satellite error component, we estimate horizontal covariances of satellite-minus-background differences, $d_b = X_{sat}^{obs} - \mathcal{H}(X^b)$, extrapolate the resulting covariance to zero distance, and compare the result with the variance of d_b. Here, our hypothesis is that background errors have no spatially uncorrelated component.

3 Data

AMSU-A (onboard NOAA-18) channels 6-9 are examined. The following radiosonde types are used: Vaisala, Sippican, VIZ, MODEM, Meisei, and Graw. We also use the 6-h. NCEP GFS forecast as the background.

4 Results

We present some selected preliminary results for 6 months of data (January-June, 2008). From the figures below, we see that both inter-channel and horizontal satellite-error correlations appear to be quite broad and more or less comparable with background-error temperature correlations. This suggests that allowing for these observation-error correlations in an analysis scheme will be beneficial.

In more detail, the results will be reported in a paper in preparation.

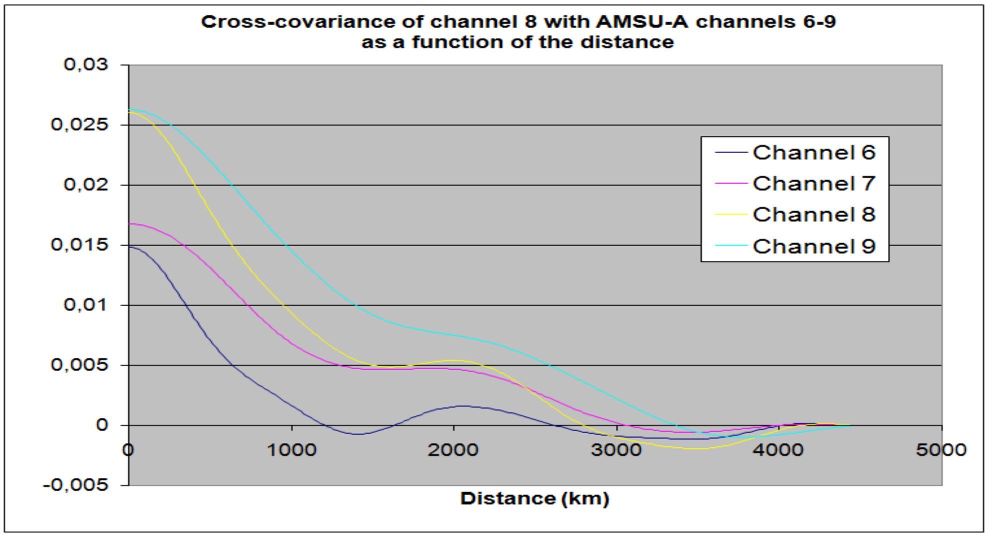
Cross-covariance of channel 8 with AMSU-A channels 6-9
as a function of the distance
0,03
0,025
0,02
0,015
0,01
0,005
0
-0,005
0
1000
2000
3000
4000
5000
Distance (km)
Channel 6
Channel 7
Channel 8
Channel 9

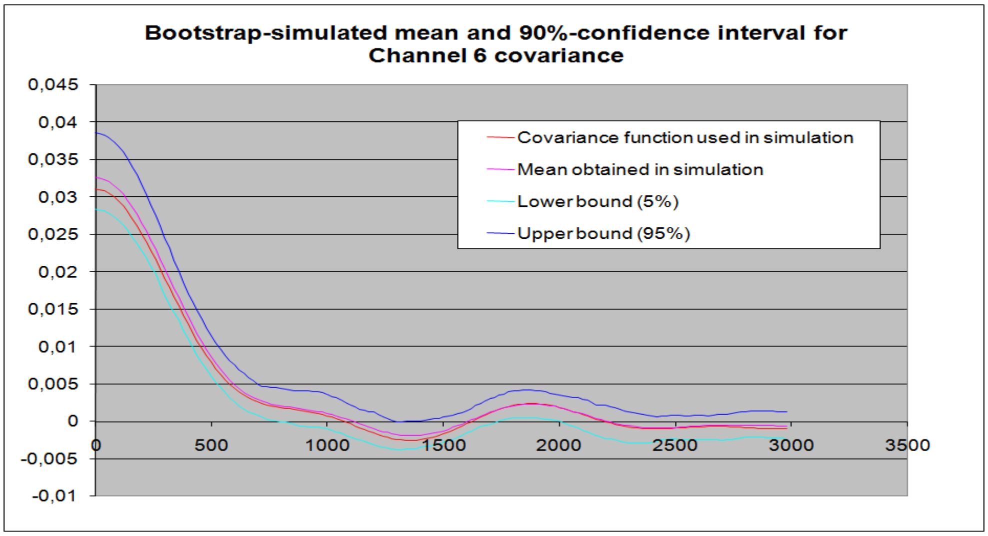
Bootstrap-simulated mean and 90%-confidence interval for
Channel 6 covariance
0,045
0,04
0,035
0,03
0,025
0,02
0,015
0,01
0,005
0
-0,005
-0,01
0
500
1000
1500
2000
2500
3000
3500
Covariance function used in simulation
Mean obtained in simulation
Lower bound (5%)
Upper bound (95%)

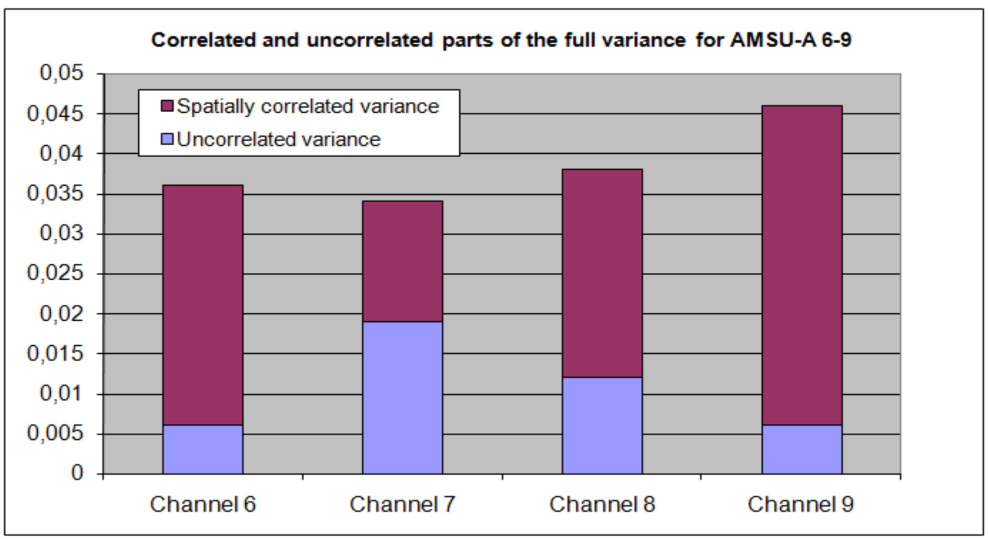
Correlated and uncorrelated parts of the full variance for AMSU-A 6-9
0,05
0,045
0,04
0,035
0,03
0,025
0,02
0,015
0,01
0,005
0
Spatially correlated variance
Uncorrelated variance
Channel 6
Channel 7
Channel 8
Channel 9

Upgrade of the Operational Mesoscale 4D-Var System at the Japan Meteorological Agency

Yuki Honda* and Ken Sawada
Numerical Prediction Division, Japan Meteorological Agency
1-3-4 Otemachi, Chiyoda, Tokyo 100-8122, Japan
(* E-mail: honda.yuuki@met.kishou.go.jp)

1. Introduction

For disaster prevention and aviation forecasting, the Japan Meteorological Agency (JMA) operates a mesoscale numerical weather prediction system known as the Mesoscale Model (MSM). The current operational mesoscale analysis setup consists of a four-dimensional variational data assimilation system based on a hydrostatic spectral model (Meso 4D-Var)(Ishikawa and Koizumi, 2002). In Honda and Sawada (2008), we announced the replacement of the Meso 4D-Var with a new JMA-NHM-based four-dimensional variational data assimilation system called JNoVA. However, this upgrade was postponed because of the deterioration of the forecast score of weak rain in summer. After various modifications and many experiments, we have succeeded in improving the JNoVA and plan to replace Meso 4D-Var with it in April 2009.

2. Improvements in the new mesoscale analysis system (JNoVA)

Detailed specifications of JNoVA are described in Honda et al. (2005). In this section, the modifications made since Honda and Sawada (2008) are briefly explained. First, the outer model has been upgraded to the latest operational forecast version, and its vertical resolution has been raised from 40 to 50 layers. Second, the moist process of the inner model has been changed; the moist convective adjustment scheme has been replaced with the Kain-Fritsch convective scheme. Although this scheme is only considered in the forward step, it contributes to the improvement of forecast trajectories. Third, a fix has been introduced for a serious bug in the handling of precipitation observation that caused a deterioration in the forecast score for weak rain in summer. Several other modifications have also been made, including the adjustment of the background error covariance matrix.

3. Performance of JNoVA

To compare the performance of JNoVA with that of Meso 4D-Var, twin experiments were conducted under almost the same conditions as the operational system in summer (2006/7/16 – 8/31) and in winter (2007/12/23 – 2008/1/23). The experimental period was changed from Honda and Sawada (2008).

The quantitative precipitation forecast (QPF) of JNoVA is better than that of Meso 4D-Var for all thresholds according to the equitable threat score (ETS) of three-hourly accumulated precipitation forecasts (Fig. 1). Even for weak rain, which is our concern here, the improvement is significant. Upper-air verification reveals that the analysis of JNoVA is better than that of Meso 4D-Var, although the impact on the forecast is quite limited (not shown). From surface verification, it is found that the root mean square errors (RMSEs) of the surface temperature in summer and the surface wind in winter are reduced, and that the scores of other surface variables are neutral (Fig. 2).

Typhoon Wukong (T0610) is picked up as a case in which JNoVA improves the forecast compared to Meso 4D-Var. Figure 3 shows a 24-hour forecast of three-hourly accumulated precipitation from the initial time of 15 UTC on 17 Aug. 2006. The improved typhoon track forecast leads to an enhancement of the precipitation pattern.

4. Summary

In general, JNoVA outperforms Meso 4D-Var, especially in the area of the quantitative precipitation forecasts. Accordingly, we plan to introduce the operation of JNoVA in April 2009 as a replacement for Meso 4D-Var. This upgrade will raise the horizontal resolution of analysis from 10 km to 5 km, while that of the inner model will also be changed from 20 km to 15 km.

References

Honda, Y., et al., 2005: A pre-operational variational data assimilation system for a non-hydrostatic model at the Japan Meteorological Agency: Formulation and preliminary results. *Q. J. R. Meteorol. Soc.*, 131, 3465-3475.

Honda, Y. and K. Sawada, 2008: A New 4D-Var for Mesoscale Analysis at the Japan Meteorological Agency. *CAS/JSC WGNE Res. Activ. Atmos. Oceanic Modell.*, 38, 01.7-01.8.

Ishikawa, Y. and K. Koizumi, 2002: One month cycle experiments of the JMA mesoscale 4-dimensional variational data assimilation (4D-Var) system. *CAS/JSC WGNE Res. Activ. Atmos. Oceanic Modell.*, 32, 0126-0127.

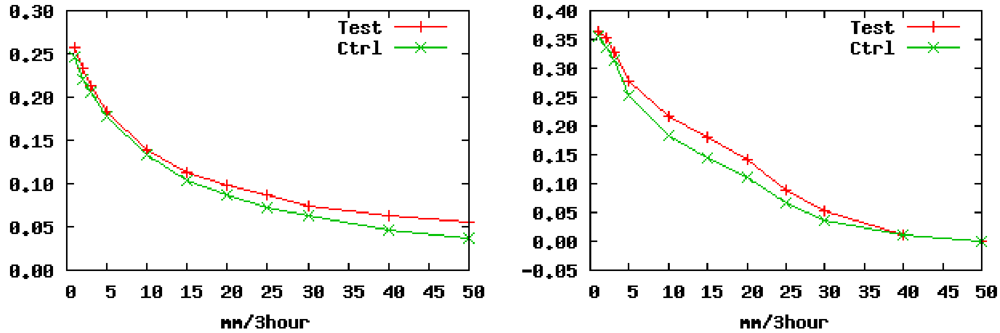

Fig. 1: Equitable threat scores of three-hourly accumulated precipitation forecasts in summer (right) and winter (left). The red and green lines show the results of JNoVA (Test) and Meso 4D-Var (CTRL), respectively. The horizontal axis is the threshold value of the rainfall amount.

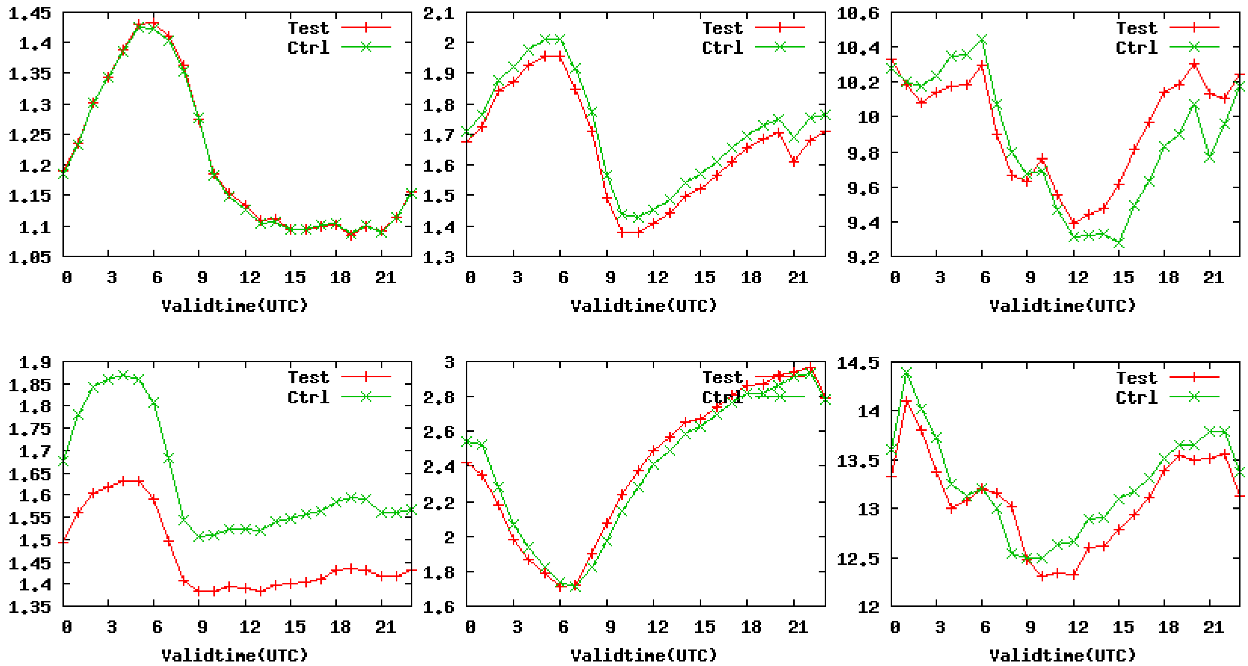

Fig. 2: Root mean square errors of wind velocity, temperature and relative humidity at the surface are shown from left to right, respectively. The upper panels are the results for summer, and the lower ones are those for winter. The line colors are the same as those in Fig. 1. The horizontal axis is the valid time, which is the real time of the forecast.

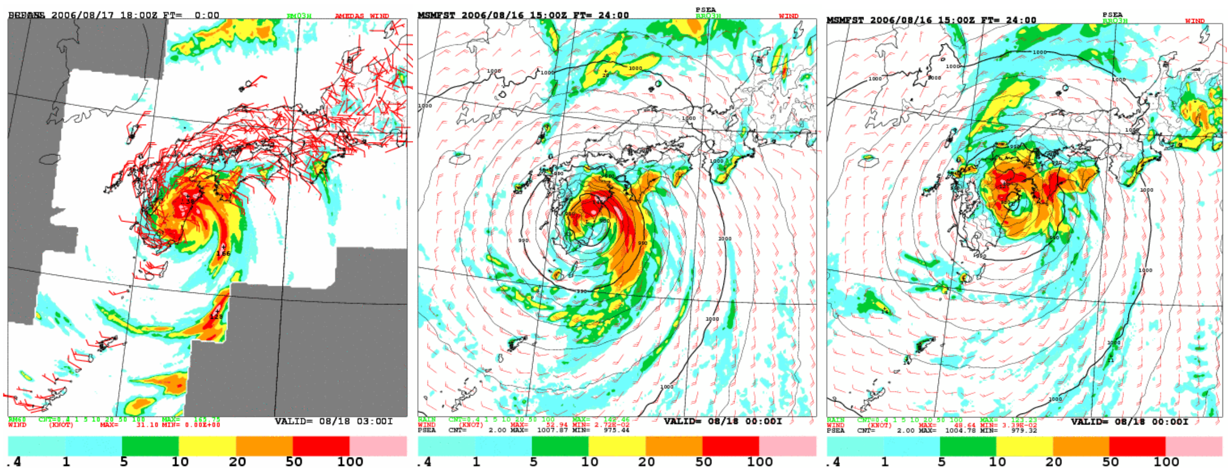

Fig. 3: Three-hourly accumulated precipitation of 24-hour forecasts from 17 Aug. 2006 at an initial time of 15 UTC. From the left, analyzed precipitation, the forecast of JNoVA and that of Meso 4D-Var are shown.

Assimilation of WV-CSRs from Five Geostationary Satellites in the JMA Global 4D-Var System

Toshiyuki Ishibashi
Numerical Prediction Division, Japan Meteorological Agency
1-3-4 Otemachi, Chiyoda-ku, Tokyo 100-8122, Japan
E-mail: ishibasi@met.kishou.go.jp

1. Introduction

The Japan Meteorological Agency (JMA) has been using clear sky radiances from the water vapor channels (WV-CSRs) of five geostationary satellites (MTSAT-1R, GOES-11 and 12, and Meteosat-7 and 9) since August 2008 in the JMA global four-dimensional variational (4D-Var) data assimilation system (DAS). WV-CSRs are generated by averaging the radiances of cloud-free pixels among several hundred pixels, such as in 16 x 16 blocks (60 km x 60 km at the nadir) in the case of MTSAT-1R. The size of the averaging area is in the same order as the horizontal resolution of the operational global forecast model. Since the original radiance data resolution is about 4 km x 4 km, the data averaging processes may reduce representativeness errors and improve the Gaussian distribution characteristics of observation error statistics through processes described by the central limit theorem (Fig. 1). WV-CSRs are sensitive to humidity in the middle to upper troposphere where there are very few observations of humidity. In general, forecast model errors of humidity are larger than those of other dynamic variables such as temperature and wind because humidity is largely dependent on moist physical sub-grid processes, which are modeled with less credibility than resolvable dry dynamics. WV-CSRs therefore provide important information in this data-sparse area.

2. Quality control of WV-CSRs

Several quality control procedures are applied to WV-CSR data in advance of 4D-Var assimilation. The data are thinned to every 2.0 degrees horizontally and every 2 hours temporally to avoid taking into account the observation error correlation, which is not considered in the JMA global 4D-Var. Those with a low percentage of clear pixels and a large standard deviation of brightness temperature are excluded because they offer low representativeness of the area. Large departure (observation minus first-guess) data are also excluded to avoid contamination from data with a non-Gaussian error statistics and to maintain tangent linearity of the observation operator. For Meteosat-7, data from near local midnight are also excluded to avoid contamination from data affected by solar stray light (Munro, 2004). The variational bias correction scheme, VarBC (Dee, 2004; Sato, 2006; Ishibashi, 2009), is applied in the 4D-Var system. The predictors of VarBC for WV-CSRs are the first-guess of brightness temperature, near-jet-level wind speed and a constant. No empirical tuning is applied to the bias correction parameters and the observation error settings.

3. Assimilation of WV-CSRs

Observing system experiments were carried out to estimate the impacts of WV-CSR data on both analysis and forecast quality for the two one-month periods of August 2007 and January 2008. Adding WV-CSRs from the five geostationary satellites reduced the dry bias of analysis and first-guess with respect to radiosondes in the mid-troposphere of the summer hemisphere (Fig. 2). The root mean square errors (RMSEs) of forecasts were significantly reduced by assimilating WV-CSRs for several variables and levels (Fig. 3). The RMSE reductions of dynamic variables such as temperature, geo-potential height and wind are interesting because the Jacobians (here defined as partial derivatives of the observation operator – the Jacobian matrix – rather than the determinant of the matrix – the Jacobian determinant) of the observation operator for WV-CSRs, RTTOV (Saunders, 2002), have major sensitivity to humidity, minor sensitivity to temperature and no sensitivity to wind. In the 4D-Var system, however, extended observation operators which include a forecast model as a time evolution operator are sensitive to these variables. The RMSE reduction of dynamic variables is due to the extended observation operators and the forward integration of the outer model. The RMSE reduction by forward integration is also explained by the sensitivity of dynamic variables to humidity in the model.

References

Dee, D. P., 2004: Variational bias correction of radiance data in the ECMWF system. *Proceedings of the ECMWF workshop on assimilation of high spectral resolution sounders in NWP*, Reading, UK, 28 June – 1 July 2004, 97 – 112.

Ishibashi, T, 2009: Implementation of a new background error covariance matrix in the variational bias correction scheme for the JMA global 4D-Var. *CAS/JSC Research Activities in Atmospheric and Oceanic Modelling*, 39, submitted.

Munro, R., C. Kopken, G. Kelly, J.-N. Thépaut and R. Saunders, 2004: Assimilation of METEOSAT radiance data within the 4D-Var system at ECMWF: Data quality monitoring, Bias correction and single-cycle experiments. Quart. J. Roy. Meteor. Soc., 130, 2,293 – 2,313.

Sato, Y., 2006: Introduction of variational bias correction technique into the JMA global data assimilation system. *CAS/JSC Research Activities in Atmospheric and Oceanic Modelling*, 37, 1 – 19.

Saunders, R., P. Brunel, F. Chevallier, G. Deblonde, S. English, M. Matricardi and P. Rayer, 2002: RTTOV-7 science and validation report.

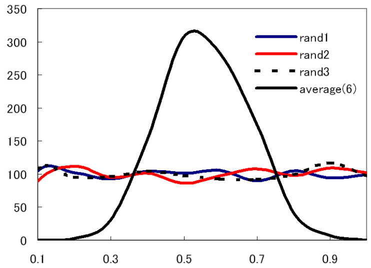

Fig. 1 Central limit theorem. The red line, blue line and black dotted line show the frequencies of random numbers generated in the range from 0 to 1. The black solid line shows the frequencies of averaged random numbers.

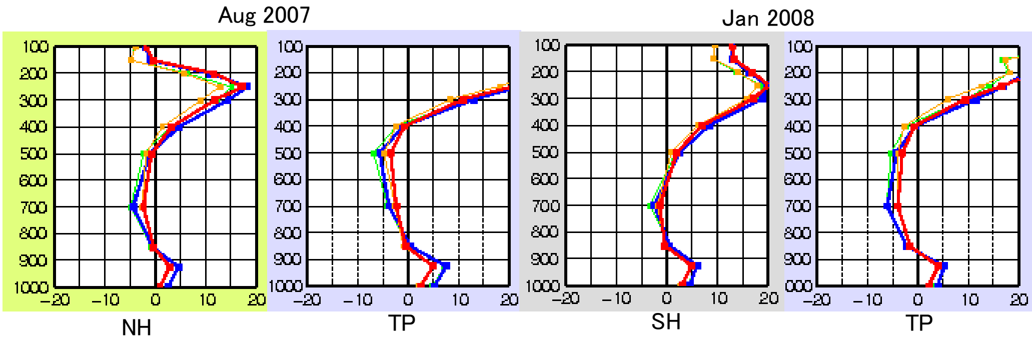

Fig. 2 The humidity biases of first guess and analysis against radiosonde observations for each experiment in the tropics and summer hemisphere. The red lines show TEST analysis, the blue lines show the TEST first guess, the orange lines show CNTL analysis and the green lines show the CNTL first guess, where TEST is the experiment with WV-CSRs and CNTL is without WV-CSRs.

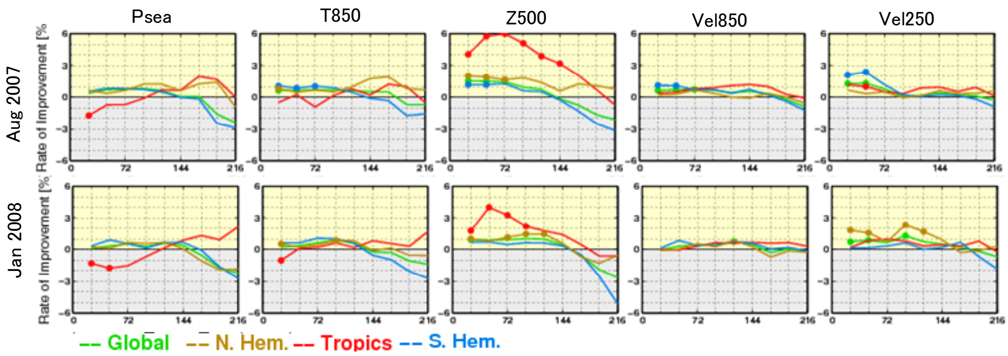

Fig. 3 Rate of improvement in the RMSE of forecast errors for sea level pressure, 850 hPa temperature, 500 hPa geopotential height, 850 hPa and 250 hPa wind velocity. The improvement rate is defined as (CNTL-TEST)/CNTL, where CNTL and TEST are the RMSE of the cycle experiment without WV-CSRs and with WV-CSRs, respectively. The dots on the score lines represent statistical significance.

Implementation of a New Background Error Covariance Matrix in the Variational Bias Correction Scheme for the JMA Global 4D-Var System

Toshiyuki Ishibashi
Numerical Prediction Division, Japan Meteorological Agency
1-3-4 Otemachi, Chiyoda-ku, Tokyo 100-8122, Japan
E-mail: ishibasi@met.kishou.go.jp

1. Introduction

The Japan Meteorological Agency (JMA) has been using a variational bias correction scheme (VarBC) operationally to correct biases of satellite radiance data in the JMA global four-dimensional variational (4D-Var) data assimilation system (DAS) since May 2006 (Sato, 2006). The background error covariance matrix (BECM) for VarBC strongly constrains the behavior of bias correction coefficients, and consequently has a large effect on the accuracy of analysis and forecasting. JMA introduced a new BECM for VarBC in the JMA global 4D-Var system in August 2008.

2. New background error covariance matrix for VarBC

The new BECM for VarBC was basically estimated from Dee (2004) and Sato (2006) by considering the balances of each term of the cost functions in 4D-Var, the amount of increment in bias correction coefficients in a single analysis, and the relationship between sampling errors and the number of the data. The new BECM for VarBC is given as follows:

$$\mathbf{B}_{\alpha,\beta} = \begin{cases} inf^2 / N_{var} & \alpha = \beta \\ 0 & \alpha \neq \beta \end{cases} \quad (1) \qquad N_{var} = \begin{cases} N / \{\log_{10}(N/N_0) + 1\} & N \geq N_0 \\ N_0 & N < N_0 \end{cases} \quad (2)$$

where $\mathbf{B}_{\alpha,\beta}$ *represents a component of the BECM for VarBC*, α *and* β *are the row and column respectively*, N *is the number of data*, $N_0 = 400$, $inf = \sigma_{system} / \sigma_d$ *represents the inflation factor*, σ_{system} *is the standard deviation (STD) of the observation errors in DAS, and* σ_d *is the STD of the observations minus the first guesses in the real data.*

The inflation factor is the ratio of the standard deviation of observation errors in DAS to the standard deviation of departures (observations minus first guesses) estimated from the real data, and absorbs discrepancies between the theoretical and real DAS. The standard deviations of the new BECM are about ten times as large as those of the old BECM; accordingly, VarBC with the new BECM (VarBC_new) represents a more adaptive bias correction scheme than that under the old BECM (VarBC_old). Analysis and forecast cycle experiments were carried out to evaluate the impact of VarBC_new on the accuracy of both analysis and forecasting in August 2007 and January 2007. The introduction of VarBC_new to DAS explicitly and statistically results in a significant reduction in analysis and forecasting errors for most areas, levels and variables (Fig. 1).

3. Properties of VarBC

Here we describe some of the properties of VarBC. First, since VarBC_new has a large BECM, a long-term three-month cycle experiment was carried out to check its stability. Fig. 2 shows the statistics of radiosonde temperature departures (observation minus first guess). There is no time-evolution of the statistics, indicating that VarBC_new is fully stable. Second, we investigated the dependencies of analysis and forecasting on other BECM settings. A cycle experiment was carried out with a very large BECM (VarBC_LG) in which the standard deviations of the BECM were about ten times as large as those of VarBC_new. The results show that VarBC_LG has a level of accuracy comparable to that of VarBC_new (Fig. 3). It can therefore be inferred that if the BECM is set to a level equal to or larger than that of VarBC_new, analysis and forecasting accuracy is maintained. This is because the number of satellite data in a single analysis is in the order of thousands, and the sampling errors become sufficiently small; accordingly, the dependency of analysis and forecasting accuracy on background bias correction coefficients is very small, and careful BECM setting is not necessary. Third, we carried out other one-month cycle experiments to compare VarBC_new with other bias correction schemes, a static scheme and an adaptive offline scheme. The experiments showed that VarBC_new has the best accuracy of the three bias correction schemes (Fig. 3).

References

Dee, D. P., 2004: Variational bias correction of radiance data in the ECMWF system. *Proceedings of the ECMWF workshop on assimilation of high spectral resolution sounders in NWP*, Reading, UK, 28 June – 1 July 2004, 97 – 112.

Sato, Y., 2006: Introduction of variational bias correction technique into the JMA global data assimilation system. *CAS/JSC Research Activities in Atmospheric and Oceanic Modelling*, 37, 1 – 19.

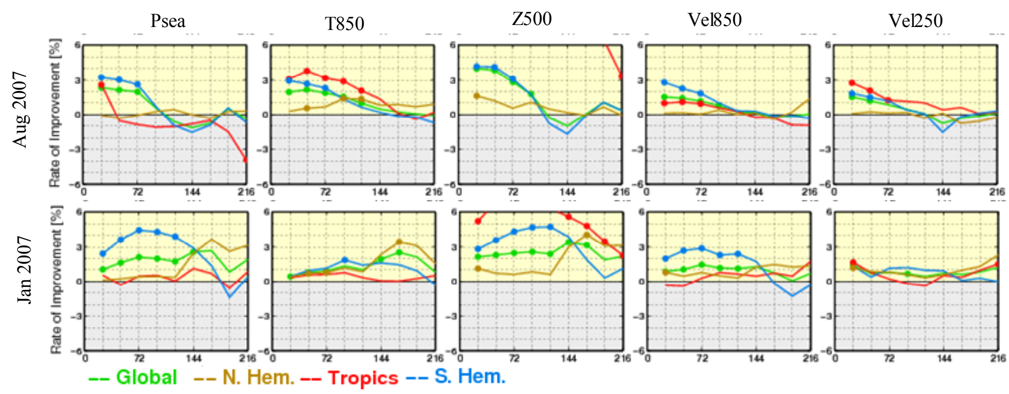

Fig. 1 Rate of improvement in the RMSE of forecast errors for sea level pressure, 850 hPa temperature, 500 hPa geo-potential height, 850 hPa and 250 hPa wind velocity. The improvement rate is defined as (CNTL-TEST)/CNTL, where CNTL and TEST are the RMSE of the cycle experiment with VarBC_old and VarBC_new, respectively. The dots on the score lines represent statistical significance.

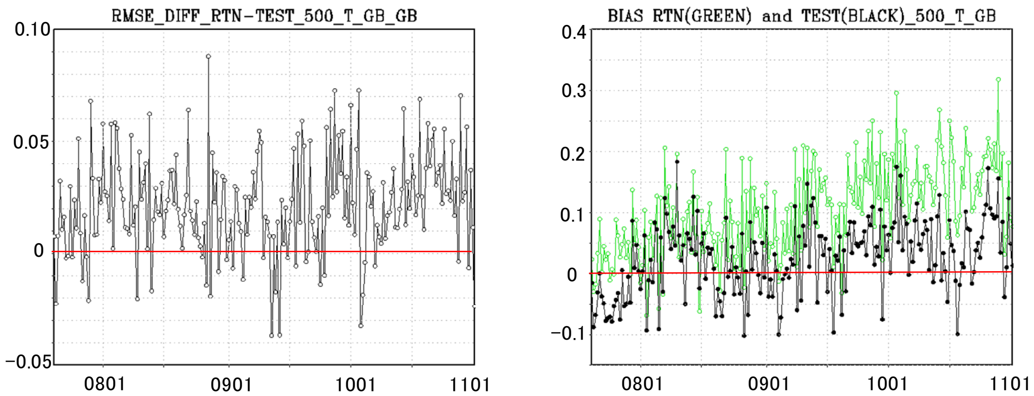

Fig. 2 The figure on the left shows differences in the RMSE of departures of radiosonde temperature at 500 hPa between VarBC_new and VarBC_old (VarBC_old minus VarBC_new). The figure on the right shows the biases of the departures. The green line is VarBC_old, and the black line is VarBC_new.

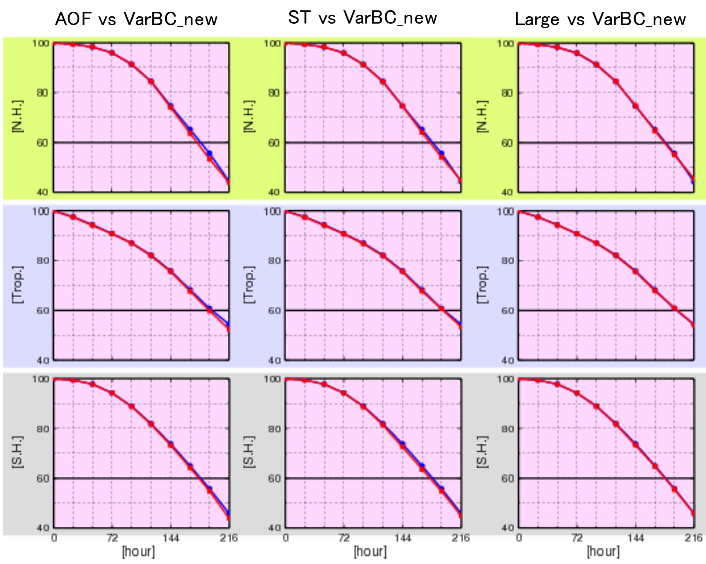

Fig. 3 Anomaly correlation (AC) of 500 hPa geo-potential height. The red lines show the AC of each cycle experiment. The leftmost column is the adaptive offline cycle, the central column is the static cycle, and the rightmost column is the VarBC_LG cycle. For each experiment, the top row is NH, the middle is TP and the bottom is SH. The blue lines show the AC of VarBC_new cycle.

Development of a Semi-Lagrangian Inner Model for Improving the Inner Resolution of the JMA Global Analysis System

Takashi Kadowaki

Numerical Prediction Division, Japan Meteorological Agency

1-3-4 Otemachi, Chiyoda-ku, Tokyo 100-8122, Japan

Email: tkadowak@naps.kishou.go.jp

In JMA, a four-dimensional variational data assimilation (4D-Var) system for the Global Spectrum Model (GSM) was introduced in February 2005 (Kadowaki, 2005; JMA, 2007). The resolution of the analysis increment was originally T63L40, and was upgraded to T106L60 in March 2006 (Narui, 2006) and to T159L60 in November 2007. T159L60 resolution is insufficient against the Tl959L60 resolution of the current forecast model. Since the resolution of the inner model is constrained by the available computational resources, it is necessary to speed up 4D-Var in order to implement higher resolution for the analysis increment. As the inner model in operational 4D-Var uses the Eulerian advection scheme, one way to accelerate calculation is to introduce a semi-Lagrangian advection scheme to the 4D-Var inner model, which is the aim of our work here.

The new inner model is based on the current JMA forecast model, which uses a two-time-level semi-Lagrangian advection scheme and a reduced Gaussian grid (Miyamoto, 2009). In the linearization of the model to make tangent-linear and adjoint models, many simplifications are performed. For instance, schemes to improve the conservative properties of mass and water vapor are ignored. The linearized fixed-point iteration involved in the semi-Lagrangian advection scheme is based on TLM2 (Polavarapu and Tanguay, 1998). Although Gauthier et al. (2007) noted that additional horizontal diffusion in the wind field was needed to avoid unstable behavior resulting from violation of the Lipschitz condition, particularly near the polar regions, no special care is taken in regard to this kind of problem, except that according to Buizza (1998), horizontal diffusion in tangent-linear and adjoint models are set to be stronger than those of the original forecast model. To examine stability near the polar regions, singular vectors were calculated using the new inner model for 40 cases in August – September 2007 with a resolution of Tl159L60, an integration time step of 1,800 seconds and an optimization time of 6 hours. The two target areas of 30°S – 90°S and 30°N – 90°N were examined. Figure 1 shows the maximum-value positions of the initial total energy of the five leading singular vectors for all cases. A few singular vectors were calculated in the vicinity of the poles, but they had neither noisy structure nor an excessive growth rate (not shown). Accordingly, the new inner model can be considered practically stable, at least for a resolution of Tl159L60 and a time step of 1,800 seconds. One reason for this stability may be the fact that our inner model uses a reduced Gaussian grid, so the increased horizontal resolution resulting from the convergence of the meridians is more moderate than that of the standard grid model. We ported most of the physical processes from the operational inner model to the new inner model and developed a new analysis system using the new version.

Forecast-analysis cycle experiments were performed for a one-month period (January 2008) using a low-resolution setting with Tl159L60 (T106L60) resolution for the analysis increment in the new (operational) analysis system and Tl319L60 resolution for forecasting. As a result, differences of analysis from both systems were found, probably resulting from the difference in gravity wave control.

Accordingly, we plan to continue the development of gravity wave control in the new system.

The new analysis system with Tl319L60 resolution and a 900 s integration time step for the inner model uses about twice as much computational time as the operational analysis system with T159L60 resolution for the inner model (the integration time step varies according to the flow) when 60 nodes of SR11000K1 are used for both systems. The computational time of the new analysis system is barely within the operational resources available at JMA; we will continue to develop the new inner model and introduce it as the next operational global analysis system as soon as it achieves comparable or better performance than the current system. The communication costs of the forecast model would present a serious problem in the future. About 35% of the computational time for the new analysis system is devoted to inter-node communications, and the ratio is almost the same for the forecast model with Tl959L60 resolution. It will be necessary to reduce inter-node communications in the forecast model itself to make the new analysis system faster.

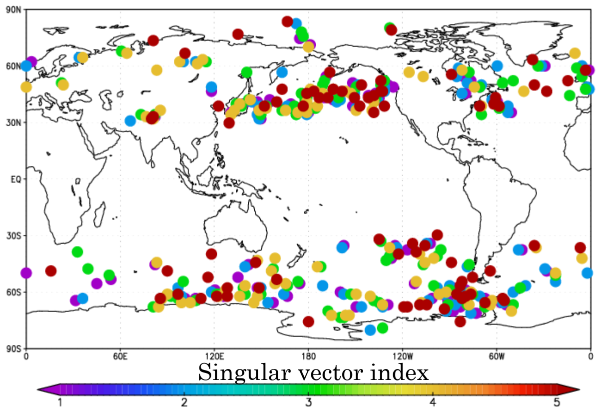

Fig 1. Maximum-value positions for the initial total energy of the five leading singular vectors (see text)

References:

Buizza, R., 1998: Impact of Horizontal Diffusion on T21, T42, and T63 Singular Vectors. *J. Atmos. Sci.*, **55**, 1069–1083.

Gauthier, P., M. Tanguay, S. Laroche, S. Pellerin, 2007: Extension of 3DVAR to 4DVAR: Implementation of 4DVAR at the Meteorological Service of Canada. *Mon. Wea. Rev.*, **135**, 2339-2354.

Gauthier, P. and J.-N. Thèpaut, 2000:Impact of the Digital Filter as a Weak Constraint in the Preoperational 4DVAR Assimilation System of Mètèo-France. *Mon. Wea. Rev.*, **129**, 2089-2102.

JMA, 2007: Outline of the operational numerical weather prediction at the Japan Meteorological Agency. Appendix to WMO Numerical Weather Prediction Progress Report. Japan Meteorological Agency, Tokyo, Japan. Available online at http://www.jma.go.jp/jma/jma-eng/jma-center/nwp/outline-nwp/index.htm

Kadowaki, T., 2005: A 4-dimensional variational assimilation system for the JMA Global Spectrum Model. CAS/JSC WGNE Research Activities in Atmospheric and Oceanic Modelling, **34**, 1-17.

Miyamoto, K., 2009: Renovation of JMA Global NWP Model. Submitted to CAS/JSC WGNE Research Activities in Atmospheric and Oceanic Modelling.

Narui, A., 2006: Changing the Resolution of the Inner Loop of Global 4D-Var at JMA. CAS/JSC WGNE Research Activities in Atmospheric and Oceanic Modelling, **35**, 1-23.

Polavarapu, S., and M. Tanguay, 1998: Linearizing iterative processes for four-dimensional data-assimilation schemes. *Quart. J. Roy. Meteor. Soc.*, **124**, 1715-1742.

The impacts of an Improved Quality Control and Ocean Emissivity Model for Microwave Radiance Assimilation in the JMA Global 4D-Var Data Assimilation System

Masahiro Kazumori
Numerical Prediction Division, Japan Meteorological Agency
E-mail: kazumori@met.kishou.go.jp

Introduction

JMA has been assimilating clear radiance data from Microwave Imagers (AMSR-E, SSM/I and TMI) in the operational global 4D-Var data assimilation system since 2006. The assimilation of these measurements provides moisture information in data-sparse areas over ocean regions and produces better typhoon forecasts and rainfall distribution [1]. The brightness temperature and its Jacobians are calculated by using a fast radiative transfer model (RTTOV-7) for the radiance data assimilation. In RTTOV-7, FASTEM-2 is used as the microwave ocean emissivity model. For the assimilation of microwave surface- sensitive channels over the ocean, the performance of the microwave ocean emissivity model within the radiative transfer model is a key element of the radiance data assimilation system. Here, the impact of improved quality control and a new microwave ocean emissivity model (FASTEM-3) in RTTOV-8 [3] were studied.

Improved quality control for microwave radiance data

Assimilation of clear radiance data is assumed in the current system. Accordingly, quality control for cloud contamination removal and bias correction of radiance data are crucial elements in the pre-process part of the assimilation. Observed brightness temperature data are categorized (clear, cloudy, rain, etc.), and only clear radiance data are selected for the assimilation. The current JMA bias correction scheme [2] corrects O-B (Observed brightness temperature minus calculated brightness temperature from the background) biases, including instrument biases, radiative transfer model biases and forecast model biases. The bias correction scheme adopts a linear regression using a number of predictors, and the regression coefficients are optimized in the 4D-Var and used in subsequent analysis. Current predictors for microwave imager data in the JMA operational system are surface wind speed, total precipitable water, incident angle, sea surface temperature (SST) and squared SST.

In this study, another quality control was added to remove cloud contamination. Retrieved cloud liquid water (CLW) values were used to estimate cloud contamination. The CLW criterion for the data rejection was set at $100 g/m^2$. The remaining biases (thin cloud and/or minimal cloud in the sensor field of view) were adjusted through variational bias correction using CLW as one of the predictors.

Experiments

Experiments for the impact study were performed using the JMA low-resolution global data assimilation system (TL319L60) and a global forecast model. The experimental period was July 20 – September 30, 2007, and the forecasts were produced from each 12 UTC initial for the test run and control run. For verification, 52 forecast cases (from 1 August to 21 September 2007) were used. In both the control run and the test run, the same JMA operational data set was used, including conventional data (surface observations, radiosonde observations and aircraft data), atmospheric motion vectors from 5 geostationary satellites and polar-orbiting satellites (Aqua and Terra), and microwave radiance data (AMSU-A, AMSU-B, MHS, SSM/I, TMI and AMSR-E). The differences between the test run and the control run were the radiative transfer model

(RTTOV-7 for the control run, RTTOV-8 for the test run), which includes a microwave ocean emissivity model change (from FASTEM-2 to FASTEM-3), and quality control and bias correction for microwave imager data.

Results

Impacts were found in the form of 850 hPa temperature forecast improvement in the tropics (Figure 1) and RMSE reductions in 500 hPa geopotential height forecasts (Figure 2). As the use of microwave imager data was limited in oceanic regions, large forecast improvements were found in the Southern Hemisphere. These experimental results indicate that the removal of cloud-contaminated data through improved quality control and the use of CLW as one of the predictors in variational bias correction were essential parts of the microwave clear radiance assimilation. The pre-process modifications and update of the radiative transfer model (including FASTEM-3 in the data assimilation) also produce improved moisture analysis, which leads to better temperature and geopotential height forecasts in the lower troposphere.

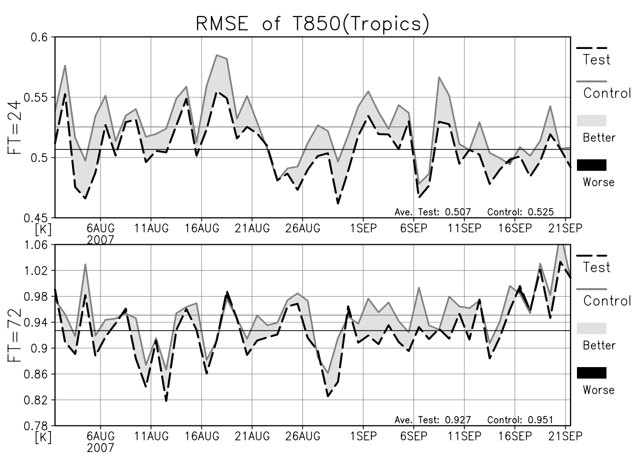

Figure 1. Time sequence of the RMSE for temperature forecasts in the tropics against the initial for one-day (upper panel) and three-day (lower panel) forecasts. The grey lines are for the control run, and the dark dashed lines are for the test run.

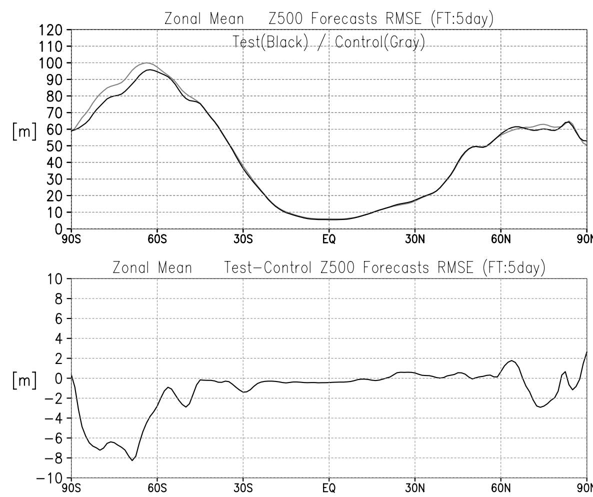

Figure 2. Zonal mean of the RMSE for five-day geopotential height forecasts (upper panel) against the initial. The black line is for the test run, and the gray line is for the control run. The lower panel shows the difference between the test run and the control run.

References

[1] Sato, Y., "Introduction of spaceborne microwave imager radiance data into the JMA global data assimilation system", *Research Activities in Atmospheric and Oceanic Modelling (WGNE Blue Book)*, Report No. 37, WMO/TD-No. 1397, Section 01, pp. 17 – 18, April 2007.
[2] Sato, Y., "Introduction of variational bias correction technique into the JMA global data assimilation system", *Research Activities in Atmospheric and Oceanic Modelling (WGNE Blue Book)*, Report No. 37, WMO/TD-No. 1397, Section 01, pp. 19 – 20, April 2007.
[3] Saunders, R. W., 2006: *RTTOV-8 Science and Validation Report.* EUMETSAT, pp. 46

Impact Study of the RTTOV-9 Fast Radiative Transfer Model in the JMA Global 4D-Var Data Assimilation System

Masahiro Kazumori
Numerical Prediction Division, Japan Meteorological Agency
E-mail: kazumori@met.kishou.go.jp

The Japan Meteorological Agency (JMA) operates a global four-dimensional variational data assimilation system for global forecasts. In this operational setup, a fast radiative transfer model (RTTOV) is utilized for satellite radiance data assimilation. Currently, RTTOV-8.7 [1] is employed in the system. However, RTTOV-9 was released by NWP SAF in March 2008 for the NWP community. Accordingly, the impact of introducing RTTOV-9 into the JMA system was investigated. RTTOV-9 includes various scientific and coding updates [2]; one important change in the model for the JMA system is the updating of the vertical interpolation method for atmospheric profiles from a user-defined level to RTTOV pre-defined levels [3]. This enables better mapping of computed temperature and moisture Jacobians on JMA global forecast model layers. Additionally, improper variation of the Zeeman effect with the strength of the earth's magnetic field for the AMSU-A upper-stratosphere channels was removed. A reduction in stratospheric temperature analysis error is expected as a result of this removal.

In order to examine the impact of the radiative transfer model updates, two assimilation experiments were performed using the JMA low-resolution global data assimilation system (TL319L60). Although the horizontal resolution is lower than that of the operational system (TL959L60), the number of the vertical layers (60) is the same in both. The observational data set used in the experiments was exactly the same as the operational one, which includes conventional data (radiosonde observations, SYNOP, BUOY and aircraft data), ocean surface wind data from QuikSCAT, atmospheric motion vectors and clear sky radiances from five geostationary satellites (MTSAT-1R, GOES-11 and 12, and Meteosat-7 and 9), MODIS polar wind data from Aqua and Terra, microwave radiance data (AMSU-A/B, MHS) from polar-orbiting satellites (NOAA-15/16/17/18, Aqua and Metop) and microwave imager radiance data from SSMI, TMI and AMSR-E. The experiments were performed for the two periods of January 2008 and September 2008. Forecasts were produced from each 12 UTC initial field during these periods. The test run used RTTOV-9.3 as the radiative transfer model, while the control run used RTTOV-8.7.

Analysis impacts related to RTTOV-9 were found in stratospheric temperature analysis. As shown in Figure 1, these impacts were large especially at high latitudes and in tropical areas. For the impact on forecasts, significant improvements of stratospheric temperature predictions were found in the winter season (S.H. in September 2008 and N.H. in January 2008), as shown in Figure 2. These improvements were also confirmed against GPS retrieval temperature data from GRACE satellites (Figure 3). Based on these findings, RTTOV-9 will be implemented in the JMA operational system after studying the impacts with high resolution model.

References

[1] Saunders, R. W., 2006: *RTTOV-8 Science and Validation Report.* EUMETSAT, pp. 46
[2] Saunders, R. W., 2008: *RTTOV-9 Science and Validation Report.* EUMETSAT, pp. 74
[3] Rochon, Y. J., L. Garand, D. S. Turner and S. Polavarapu, 2007: Jacobian mapping between vertical coordinate systems in data assimilation, *Q. J. Roy. Meteorol. Soc*. **133** *1547 – 1558*.

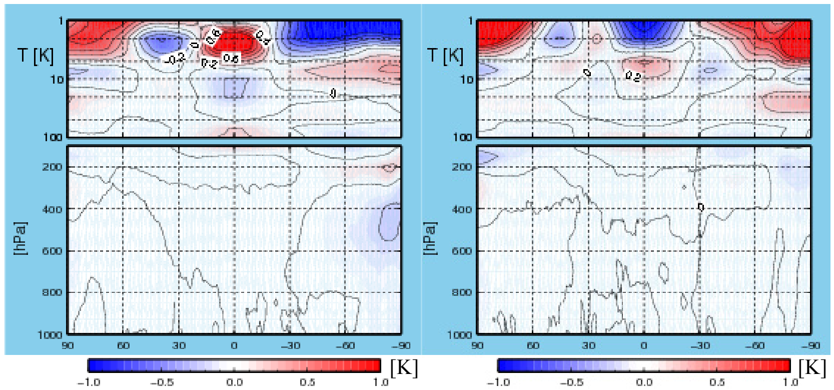

Figure 1. Monthly mean differences in zonal mean temperature between the test and control runs (Test – Control). The figure on the left is for the monthly mean of January 2008, and the one on the right is for that of September 2008.

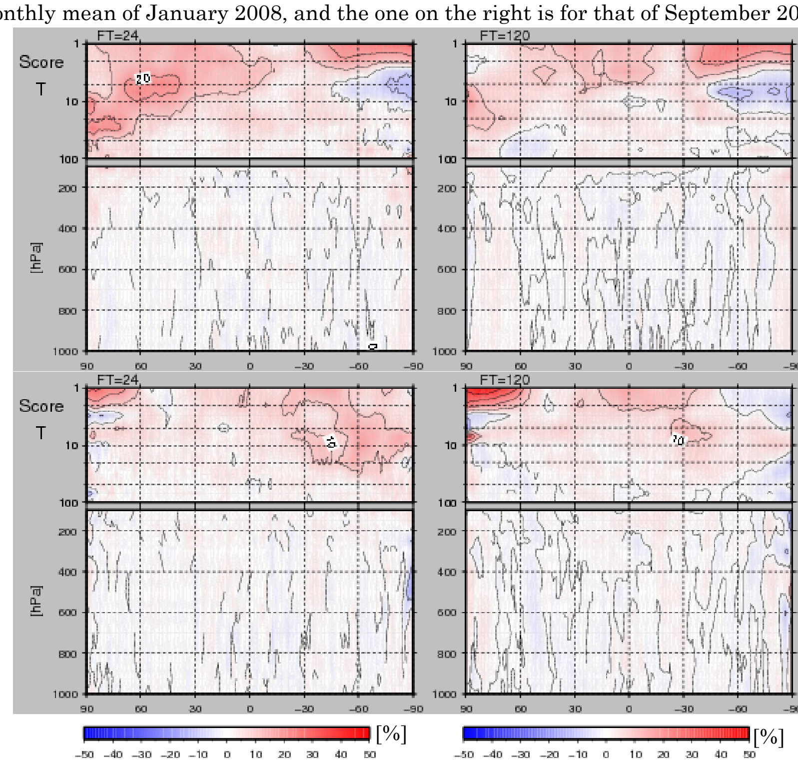

Figure 2. Zonal mean of improvement ratio for temperature forecast against the initial field. The upper two panels are for January 2008, and the lower ones are for September 2008. Those on the left are for 24-hour forecast and those on the right are for 120-hour forecast.

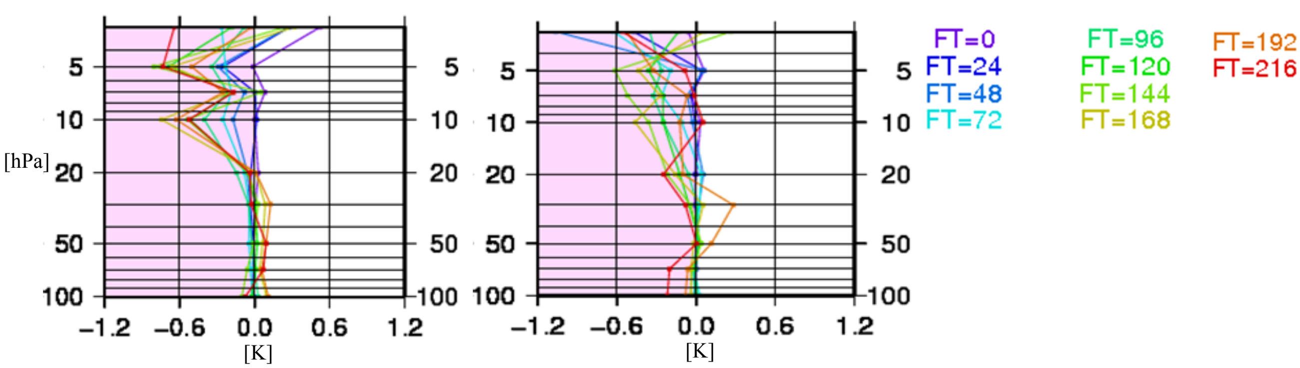

Figure 3. Difference in the standard deviation of temperature forecast profiles against GPS (GRACE) retrieval temperature profiles between the test and control runs (Test – Control). The panel on the left is for the Northern Hemisphere in January 2008, and that of the right is for the Southern Hemisphere in September 2008.

Assimilation Experiments on Pre-processed DMSP-F16 SSMIS Radiance Data in the JMA Global 4D-Var Data Assimilation System

Masahiro Kazumori
Numerical Prediction Division, Japan Meteorological Agency
E-mail: kazumori@met.kishou.go.jp

The Special Sensor Microwave Imager Sounder (SSMIS) on board the Defense Meteorological Satellite Program (DMSP) F-16 spacecraft observes radiance from the atmosphere and the surface of the earth. The SSMIS instrument is the successor to the DMSP/Special Sensor Microwave Imager (SSMI) series, and is scheduled to be on board from DMSP F-17 to F-20 in the transition period from the Polar Operational Environmental Satellite (POES) to the National Polar-orbiting Operational Environmental Satellite System (NPOESS). In addition to SSMI surface-sensitive channels ranging from 19 to 37 GHz, SSMIS has atmospheric temperature sounding channels in the 50 – 60 GHz range. Atmospheric temperature information from SSMIS is expected to be useful in Numerical Weather Prediction (NWP) in the same way as AMSU-A sounding channels.

However, calibration and validation of DMSP-F16/SSMIS revealed sensor problems with SSMIS measurements after launch [1]. The main reasons for this were reflector emission/ scattering and solar contamination in the warm calibration target. These issues caused systematic bias and noise at the temperature sounding channels and made it difficult for the data to be used in NWP. To address these problems, the UK Met Office developed a pre-process for the SSMIS radiance data [2], and has been distributing the pre-processed results to the NWP community since July 2006. JMA has been receiving this data since May 2007.

The quality of the pre-processed SSMIS data was examined, and assimilation experiments to investigate their impact on analysis and forecast were performed in the JMA system. Figure 1 shows an example distribution of pre-processed SSMIS temperature sounding data in a six-hour global assimilation time window. A total of 4,000 to 5,000 points data are available in 160-km grid box data thinning. After the removal of cloud-contaminated data, O-B (Observed brightness temperature minus calculated brightness temperature from the background) statistics showed that the qualities of the pre-processed SSMIS temperature sounding channels were comparable with those of Metop AMSU-A (Figure 2) and were acceptable for the data assimilation. Low-resolution (TL319L60) assimilation experiments demonstrated significant improvement of forecast accuracy in terms of anomaly correlation at 500 hPa geopotential height in the Southern Hemisphere when the data were added to the full operational observation data set in the JMA global data assimilation system (Figure 3). Based on these results, high-resolution (TL959L60) assimilation experiments are planned toward the use of the data in JMA's operational system.

References

[1] D. B. Kunkee, G. A. Poe, D. J. Boucher, S. D. Swadley, Y. Hong, J. E. Wessel, and E. Uliana, "Design and evaluation of the first Special Sensor Microwave Imager/Sounder," *IEEE Trans. Geosci. Remote Sens.*, vol. 46, no. 4, pp. 863 – 883, Apr. 2008.

[2] W. Bell, S. J. English, B. Candy, N. Atkinson, F. Hilton, N. Baker, S. D. Swadley, W. F. Campbell, N. Bormann, G. Kelly, and M. Kazumori, "The assimilation of SSMIS radiances in numerical weather prediction models," *IEEE Trans. Geosci. Remote Sens.*, vol. 46, no. 4, pp. 884 – 900, Apr. 2008.

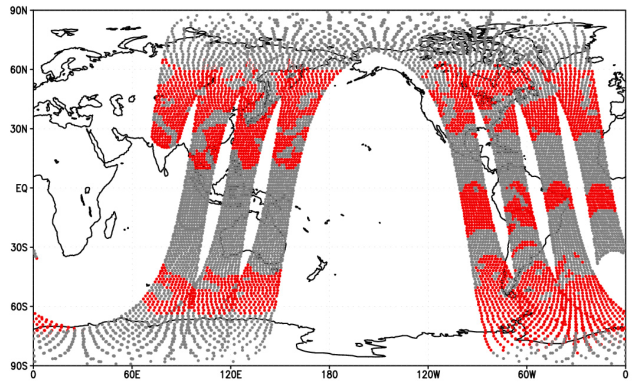

Figure 1. An example of available data distribution of SSMIS temperature sounding channels after pre-processing by the UK Met Office in a six-hour assimilation time window. The red points indicate locations where data are available.

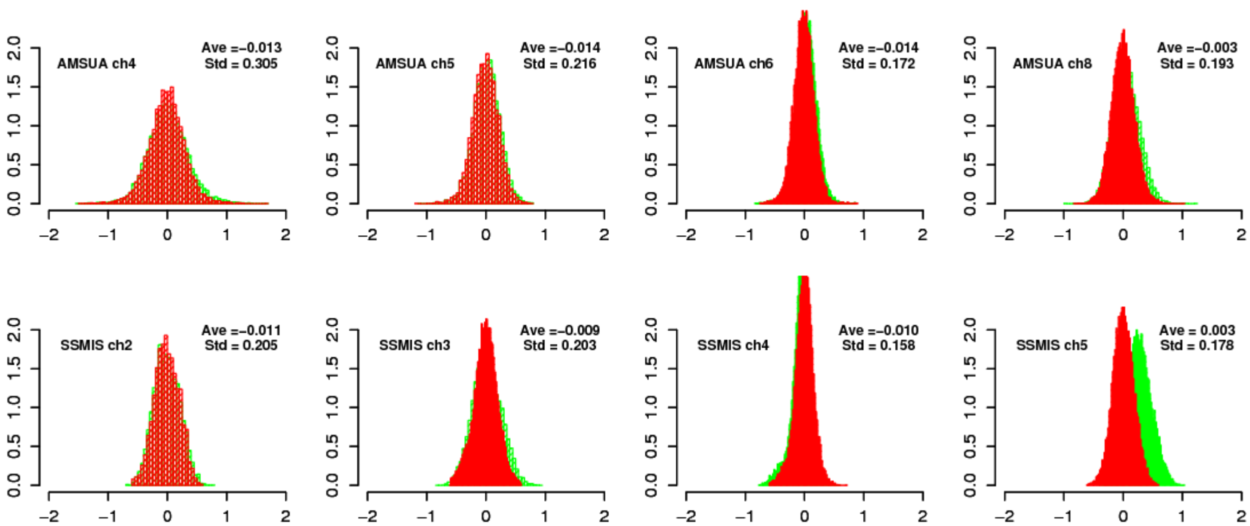

Figure 2. O-B statistics for Metop AMSU-A (ch. 4, 5, 6, 8) and SSMIS (ch. 2, 3, 4, 5). The red histograms are for after air-mass bias correction, and the light green ones are for before the bias correction.

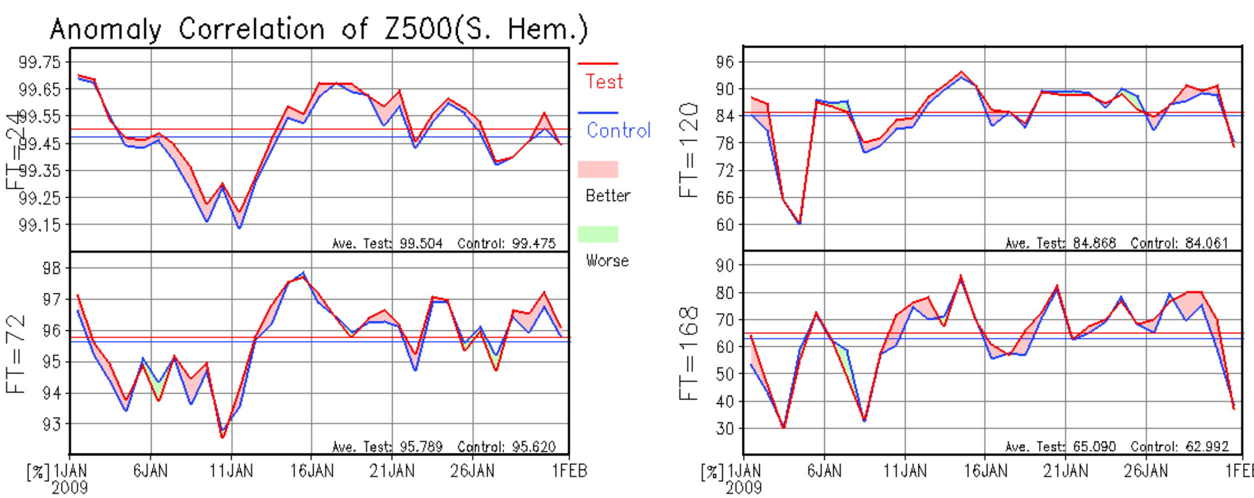

Figure 3 Time sequences of anomaly correlation at 500 hPa geopotential height in the Southern Hemisphere (FT=24, 72, 120, 168). The red lines are for the test run (with SSMIS), and the blue ones are for the control run (without SSMIS). Pink shading indicates improvement, and light green shading indicates degradation of forecast accuracy.

JMA's Total Energy Singular Vector Sensitivity Guidance for Adaptive Observations during T-PARC 2008

Takuya KOMORI [1]*, Ryota SAKAI [1], Hitoshi YONEHARA [1], Kiyotomi SATO [1],
Takemasa MIYOSHI [2], Munehiko YAMAGUCHI [1, 3], Tetsuo NAKAZAWA [4]

1: Numerical Prediction Division, Japan Meteorological Agency, Tokyo, Japan
2: University of Maryland, College Park, Maryland, USA
3: University of Miami, Miami, Florida, USA
4: Typhoon Research Department, Meteorological Research Institute, Tsukuba, Japan
Email: komori@met.kishou.go.jp

1. INTRODUCTION

The Japan Meteorological Agency (JMA) performed sensitivity analyses and supplemental observations of tropical cyclones (TCs) as a part of the THORPEX Pacific Asian Regional Campaign (T-PARC). The observations were conducted with the aim of improving numerical weather prediction (NWP) performance, especially for TC track forecasts. The supplemental observational data included dropsonde deployment by manned Falcon aircraft, enhanced radiosonde observations by research vessels and fixed observation stations, and MTSAT rapid-scan operations. To provide guidance for the observations (referred to as adaptive observations), sensitivity analyses were performed using the singular vector (SV) method with the moist total energy (TE) metric evaluated at the initial and final times of the optimization time interval (TESV).

2. JMA'S SENSITIVITY ANALYSIS SYSTEM

For effective decision-making in adaptive observations using information from sensitive areas, a two-day lead time is necessary to plan each observation. Accordingly, sensitivity analysis was performed for the forecast fields (T+24 h and T+48 h) of the operational Global Spectral Model (GSM) at TL959L60 resolution. In the calculation of TESV, four target areas were defined in the western North Pacific. Three of these were fixed target areas (referred to as GUAM, TAIWAN and JAPAN) for daily analysis, and the other was an adaptive target area (referred to as MVTY) in the vicinity of the TC location. Figure 1 illustrates the four target areas for a typhoon. The fixed areas were useful for intercomparison between different providers, while the adaptive target area was more adequate for each TC case. The MVTY target region was automatically defined according to the TC position forecasted by the operational GSM. The norm used for measuring the amplitude of perturbations at both the initial and final times was based on moist TE as described by Ehrendorfer et al. (1999). The SVs calculated for all target areas were often defined as moist SVs because moist processes – including large-scale condensation and deep convection – were implemented in the tangent linear and adjoint models at T63L40 resolution for the global domain. The specifications of the sensitivity analysis for T-PARC are shown in Table 1.

3. SENSITIVITY GUIDANCE AND ADAPTIVE OBSERVATIONS FOR TYPHOON SINLAKU

The adaptive observations were performed for Typhoon Sinlaku, the 13th named tropical cyclone in the western North Pacific of 2008. Figure 2 indicates the supplemental observation points overlaid on the sensitive area for the MVTY region that was calculated from the two-day forecasted field valid at the time of special observations at 00 UTC on 11 September 2008. The highly sensitive area was defined as a region of large vertically integrated TE normalized by the maximum value of TE in the global domain.

To estimate the usefulness of TESV structures, sensitive areas from two- and one-day forecast fields were compared to those of the analysis field using the similarity index (Buizza, 1994). This index is equal to 1.00 when the two TESVs are identical. Table 2 denotes the results calculated for the observation at 00 UTC on 11 September 2008 (shown in Figure 2). The value between the leading TESV from the two-day forecast field and that of the analysis field is 0.85, indicating good usability for the TESV provided in advance.

The T-PARC observational data were distributed through the Global Telecommunication System to enable their use in operational NWP systems worldwide. Figure 3 outlines the results of the extra observational data denial experiment; it shows that, without special observation data assimilated into the NWP system, GSM failed to adequately forecast the recurvature of Sinlaku. In the interests of natural disaster reduction and mitigation, good forecast skill for TC recurvature as seen in this example is of great importance to people living in Pacific basin countries, including Japan. Other results of the data denial experiments are described by Yamashita et al. (2009).

Table 1. Specifications of the sensitivity analysis system for T-PARC

Forecast domain	Global			
Method	Singular vector			
Inner model resolution	Spectral triangular truncation at 63 wave numbers (T63), 40 levels (from surface to 0.4 hPa)			
Norm	Moist total energy			
Target area	GUAM (05 – 25N, 135 – 155E)	TAIWAN (18 – 30N, 117 – 140E)	JAPAN (25 – 45N, 120 – 150E)	*MVTY
Optimization time interval	48 hours			24 hours
Physical process	**Full physics			

*The MVTY target region is automatically defined in the vicinity of each TC position forecasted by the operational GSM.

**Full physics: Initialization, horizontal diffusion, surface turbulent diffusion, vertical turbulent diffusion, gravity wave drag, long wave radiation, large-scale condensation and deep convection

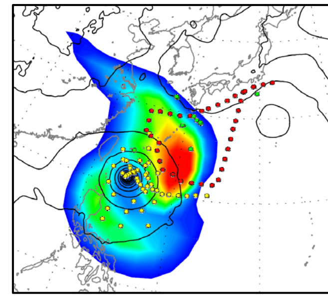

Figure 2. The sensitive area (shaded) calculated from the two-day forecasted field valid for special observations at 00 UTC on 11 September 2008. Extra observation points for upper-soundings by JMA research vessels and ground observatories (green points), dropsondes released by Falcon aircraft (red) and those released by other planes (yellow) are overlaid on the sensitive area.

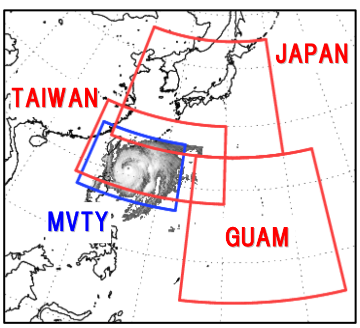

Figure 1. Schematic map showing the four target areas (defined in Table 1)

Table 2. Similarity index for the leading SV

Similarity	Two-day lead time	One-day lead time	Analysis
Two-day lead time	1.00	0.88	0.85
One-day lead time		1.00	0.93
Analysis			1.00

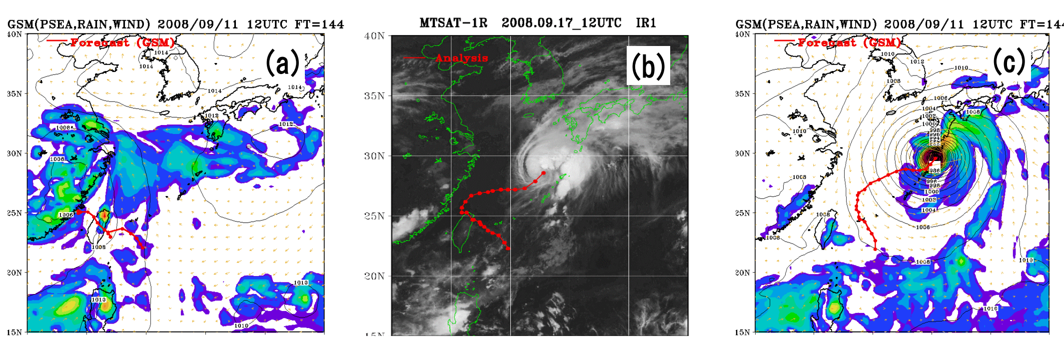

Figure 3. Impact study for Typhoon Sinlaku at 12 UTC on 11 September 2008. Forecasts by the operational GSM with and without supplemental observations are shown by the red lines (typhoon tracks) and shaded areas (rain fields) in (a) and (c), respectively. The track analyzed by the RSMC Tokyo-Typhoon Center is plotted on the MTSAT image in (b).

REFERENCES

Buizza, R., 1994: Sensitivity of optimal unstable structures. *Quart. J. Roy. Meteor. Soc.*, **120**, 429 – 451.

Ehrendorfer, M., R. M. Errico, and K. D. Raeder, 1999: Singular-Vector perturbation growth in a primitive equation model with moist physics. *J. Atmos. Sci.*, **56**, 1,627 – 1,648.

Yamashita, K., Y. Ohta and T. Nakazawa, 2009: An Observing System Experiment on the Special Observations of T-PARC for Typhoons Sinlaku and Jangmi using the Operational NWP System at JMA. *CAS/JSC WGNE Research Activities in Atmospheric and Oceanic Modelling*, **41**, submitted.

Sensitivity Analysis using the Mesoscale Singular Vector

Masaru Kunii and Kazuo Saito

Meteorological Research Institute, Tsukuba, Ibaraki 305-0052, Japan; mkunii@mri-jma.go.jp

In September 2008, a sensitivity analysis experiment using the mesoscale singular vector (MSV) was performed by MRI/JMA to support the THORPEX Pacific Asian Regional Campaign (T-PARC). The mesoscale singular vector method has been developed for the use of the initial perturbation of mesoscale ensemble prediction at MRI/JMA. MSVs are calculated using a tangent linear model (TLM) and an adjoint model (ADM) of the JMA non-hydrostatic model variational data assimilation (JNoVA) system (Honda *et al.* 2005). In TLM and ADM, some parts of the nonlinear model are simplified, such as large-scale condensation and moist convective adjustment used in moist processes. To solve the eigenvalue problem the Lanczos algorithm with Gram-Schmidt re-orthogonalization is adopted. To define the perturbation growth, the total energy norm is used, considering a moisture term.

The model domain and the targeted area of this experiment appear in Fig.1. The targeted area is fixed to the 27.5-42.5N, 125.0-145.0N, which is independent of a typhoon position. The horizontal resolution is 40 km and the optimization time is set to 12 hours to ensure the validity of the tangent linear approximation. In the near-real time operation, the 24-hour forecast of the JMA Global model (GSM; TL959L60) is used for initial condition to calculate MSVs, so that leadtime of about 14 hours is kept prior to the observation time of T-PARC.

Here a result for the case of TY0813 (SINLAKU), which caused a torrential rainfall at Kyushu district, is introduced. MSVs-based sensitivity areas for the typhoon were located in the right side to the moving direction of the typhoon, which was dominated by the potential energy components in the mid-lower troposphere (Fig.2). Compared with Global singular vectors (not shown), MSVs reflect the small scale structures which affect mesoscale disturbances rather than synoptic events including the track of tropical cyclones.

To examine the validity of the sensitivity analysis based on MSV, a data denial experiment over sensitivity area was conducted. This experiment systematically excludes all observations in the sensitivity area. Data assimilation and forecast experiments were performed using JMA Meso-4DVar and NHM. Figure 3 shows the difference of analysis field between the denial experiment (DENIAL) and the control experiment (CNTL). The denial experiment changed the water vapor fields over sensitivity area, which is similar to SVs, especially 4th SV (Fig.3(c)). Figure 4 shows the subsequent model forecast results using DENIAL and CNTL analysis as initial fields respectively. The data denial experiment shows that the exclusion of observations over the sensitivity region has an impact on forecast fields, however deterioration of forecast accuracy was not large because the difference of analyzed moisture fields with and without the data was small in this case. The difference of forecast fields at FT=12 in data denial experiments is conspicuous near the typhoon center, which does not necessarily consistent with the locations of final MSVs (not shown). This discrepancy is probably attributable to the track error (about 100 km) in the GSM 24-hour forecast used as the initial condition to calculate MSVs. To further assess the propriety of the MSV-based sensitivity region, OSSE on water vapor fields around typhoon center is necessary.

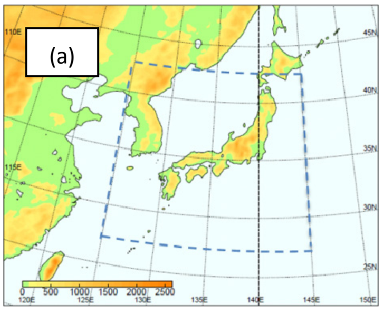

Fig.1. Model domain and the target area (broken line).

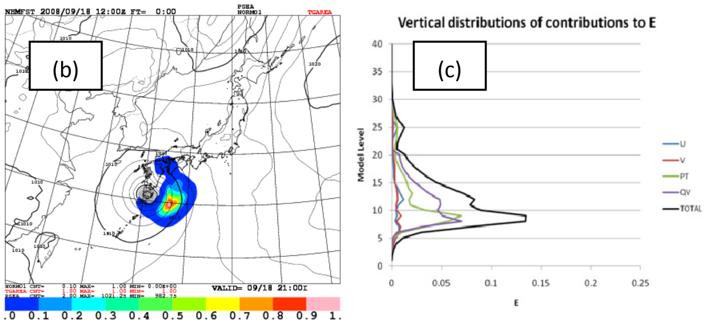

Fig.2. (a) Horizontal distribution of 1st MSV, (b) Vertical distributions of contributions to total energy norm. Observational time is 12 UTC on 18 September 2008.

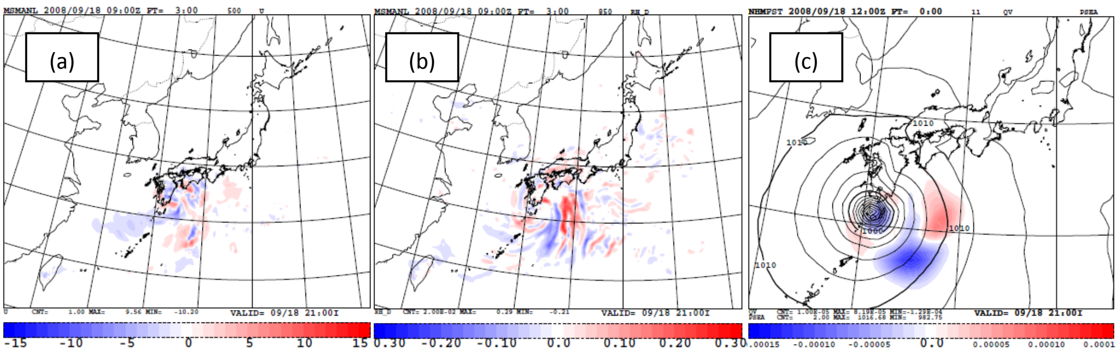

Fig.3. (a) Difference of analysis field between DENIAL and CNTL, zonal wind at 500hPa, (b) Same as in (a) but relative humidity at 850hPa, (c) QV of 4th MSV (z=1.46 km).

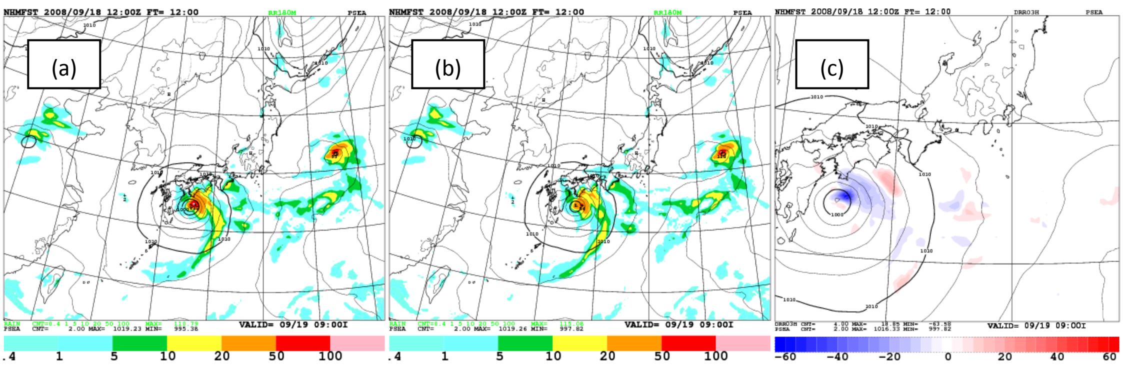

Fig.4. 3-hour accumulated precipitation (color) and SLP (contour) at 00 UTC on 19 September. (a) CNTL, (b) DENIAL, (c) difference of 3-hour accumulated precipitation between DENIAL and CNTL.

References

Honda, Y. et al., 2005: A pre-operational variational data assimilation system for a nonhydrostatic model at Japan Meteorological Agency: Formulation and preliminary results. *Quart. J. Roy. Metor. Soc.*, **131**, 3465-3475.

Developments in the context of the Concordiasi project in Antarctica for the International Polar Year (IPY)

Florence Rabier, Aurélie Bouchard, Vincent Guidard, Fatima Karbou, Stéphanie Guedj

CNRM-GAME, Météo-France and CNRS
42 av Coriolis, 31057 Toulouse, France
Florence.Rabier@meteo.fr

Within the framework of the IPY, the Concordiasi project (http://www.cnrm.meteo.fr/concordiasi/) will make innovative observations of the atmosphere above Antarctica in order to
* Enhance the accuracy of weather prediction and climate records in Antarctica through the assimilation of in-situ and satellite data
* Improve our understanding of microphysical and dynamical processes controlling the ozone content of the polar air masses, by providing the first quasi-Lagrangian observations of ozone and particle content, in addition to an improved characterization of the polar vortex dynamics.
A major Concordiasi component is a field experiment during the Austral springs of 2008 and 2009. The field activities are based on a constellation of up to eighteen long duration stratospheric balloons deployed from the McMurdo station. Six of these balloons will carry GPS receivers and in-situ instruments measuring temperature, pressure, ozone, and particles. All the balloons are capable of releasing dropsondes on demand for measuring atmospheric parameters. Finally, radiosounding measurements are collected at various sites, including the Concordia station.
Studies have been performed on how to improve the estimation of microwave emissivity over Antarctica, following the approach developed in Karbou et al. (2006). Feasibility studies have also been undertaken to improve our knowledge of the variability of surface emissivity over Antarctica. Surface emissivity retrievals in these studies make several assumptions about surface conditions. For example, the land surface emissivity is usually derived from satellite observations assuming that the surface is flat and specular. In fact, snow significantly scatters microwaves, and a specular assumption for the surface may introduce biases for observations from scan-track instruments such as AMSU-A and AMSU-B. To study the sensitivity of surface properties in retrievals, land surface emissivities at AMSU window frequencies have been calculated using specular, lambertian, and intermediate surface reflectivities. It has been found that emissivities derived at 50 GHz and from observations close to nadir are rather sensitive to assumptions about the surface. Simulations of brightness temperatures at sounding channels have been made and have been compared with observations. For the simulations, the land surface emissivity at the closest window channel, in frequency, has been assigned to each sounding channel. For instance, emissivities derived at 50 GHz have been assigned to AMSU-A temperature channels (50-60 GHz) and emissivities derived at 89 GHz have been assigned to AMSU-B humidity channels. It has been found that the best results are obtained when the surface is assumed to have 50% specular reflection and 50% lambertian reflection. Figure 1 shows the correlations between observations and simulations for AMSU-A channel 4 (52.3 GHz). Results are plotted for a control experiment, for an experiment that uses land surface emissivities assuming the surface to have specular reflection and for an experiment that uses land surface emissivities assuming the surface to have specular reflection and lambertian reflections (50% each). In the control experiment, the land surface emissivity was estimated using the empirical version of Grody (1988) and Weng et al. (2001) models for AMSU-B and AMSU-A observations respectively. Observations and simulations correlate much better after inclusion of a surface emissivity that varies in space and time. More in depth studies are planned in order to examine the impact of even more realistic descriptions of Antarctica surface emissivity on analysis and forecast skill.

As far as the assimilation of advanced infrared sounders is concerned, cloud detection is also an issue. The cloud detection scheme (McNally and Watts, 2003) used operationally at Météo-France, was validated with respect to MODIS information over Antarctica and sea ice. Then channels peaking in the stratosphere and upper troposphere were selected for assimilation over land and sea-ice, in addition to channels being used over open sea.

To take advantage of these microwave developments, a new assimilation suite, using additional AMSU-A and AMSU-B data, and also more AIRS and IASI channels over land and sea-ice, has been tested. Scores over the Southern Hemisphere show a better model performance (Figure 2).

Developments will continue and in-situ data obtained from September to November 2009 will be most helpful to validate our satellite data assimilation over these regions.

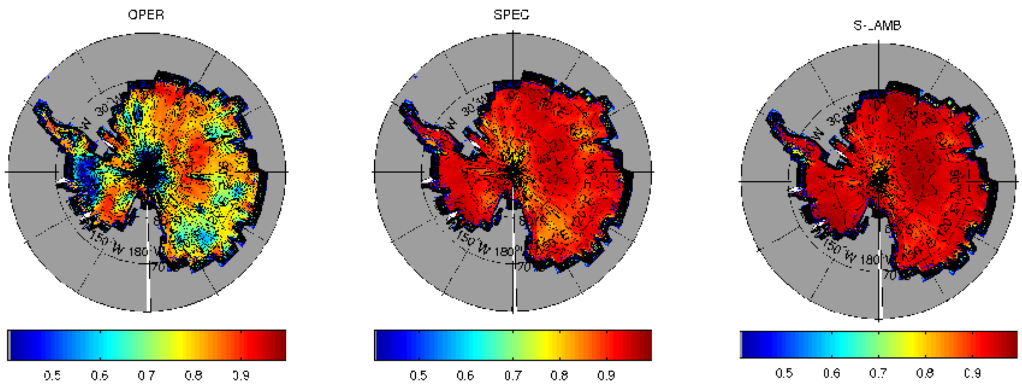

FIG. 1. Map of correlations between observations and simulations of AMSU-A channel 4 (52.3 GHz) for January 2007. Results are shown for a control experiment (left-hand panel), an experiment in which the land surface emissivity has been estimated assuming the surface to have specular reflection (middle panel), and an experiment in which the land surface emissivity has been estimated assuming the surface to have specular and lambertian reflection (50% each) (right-hand panel). The correlations have been computed taking into account data in grid cells of 2°x2° size.

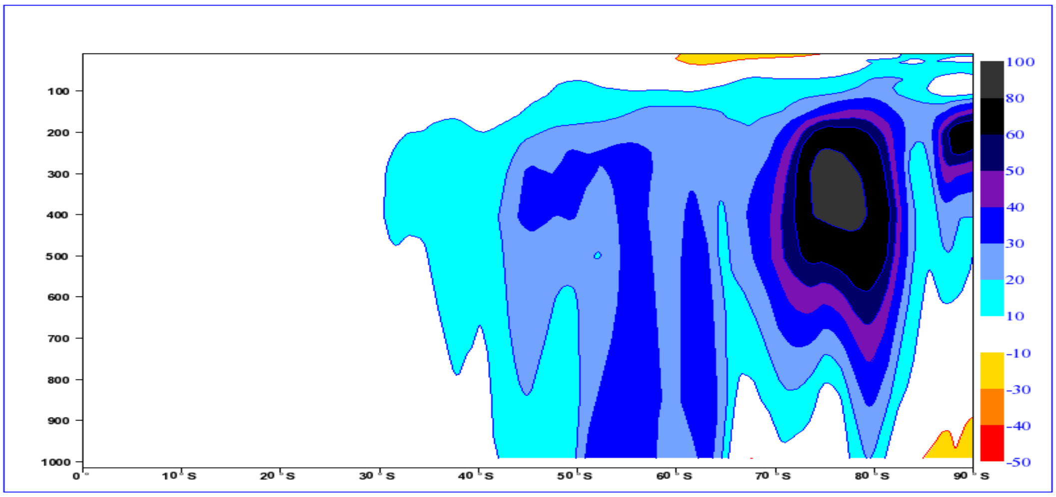

FIG. 2. Statistics of the differences in root-mean-square errors between a version of the ARPEGE model assimilating the same observations as in operations and a version of the model using more satellite data over Antarctica. The statistics are shown for the geopotential errors of the 72-h forecasts over a period of three weeks in July 2007, averaged latitudinally. Blue (resp. yellow) colours indicate that the additional AIRS, IASI and AMSU observations over Antarctica have improved (resp. degraded) the forecasts.

Current developments in global and regional data assimilation at Météo-France

Florence Rabier, Claudia Faccani, Nadia Fourrié, Elisabeth Gérard, Vincent Guidard, Fatima Karbou, Patrick Moll, Christophe Payan

CNRM/GAME, Météo-France and CNRS
42 av Coriolis
31057 Toulouse
France
Florence.Rabier@meteo.fr

Variational assimilation is a good algorithmic framework for an efficient use of observational data of different kinds. In particular, data from the AMSU-A, AMSU-B/MHS, HIRS, AIRS and SSM/I satellite instruments are assimilated under the form of raw brightness temperatures and scatterometer wind observations are used over open sea. Developments in terms of data usage which took place in 2008 are summarized below.

Very recently, IASI data from the European MetOp satellite have been inserted (1 July 2008). IASI was launched in October 2006, onboard the polar orbiting European satellite MetOp. This new instrument is a Michelson interferometer which sounds a wide spectrum in the infrared region. Similarly to all satellite-based radiances, IASI data have to be bias corrected (e.g. from viewing geometry or air mass induced biases) before being assimilated. The variational bias correction is a method that continuously adapts to possible variations of the bias; it has been used in operations since February 2008 and satisfactorily handles biases in IASI and other satellite data. Since July 2008, 50 IASI channels are assimilated over open sea in operations, both in the global model ARPEGE and the regional model ALADIN; they bring information on atmospheric temperature. The subsequent impact on forecasts is largely positive up to 4-day range in extra-tropical regions, especially in the Southern Hemisphere.

Already used at high-resolution in the ALADIN model, the radiances observed by Meteosat Second Generation (MSG) are now assimilated into the global operational model ARPEGE as Clear Sky Radiances (CSR produced by EUMETSAT), with a horizontal sampling of 250km similarly to the other satellite data. The impact of these data is relatively small but always positive, especially over Europe, and these observations contribute to the observation network above our area of interest.

The ocean surface wind measured by scatterometry is retrieved with an ambiguity about the direction, resolved with the model background. Taking into account the 4-most likely directions of the SeaWinds scatterometer (instead of 2) improves the measurement quality (mainly in dynamically active areas), similar to that of the new data from ASCAT scatterometer, for which only two directions can be considered. The combination of these two instruments together with the AMI scatterometer (similar to ASCAT) is the best observing system for the ocean surface winds (1.2 $m.s^{-1}$ in terms of standard deviation vector), with an almost global coverage every 6 hours and therefore an improved monitoring of tropical cyclones.

Radiosondes are to date of prime importance for Numerical Weather Prediction. However, these observations are known to be biased and therefore need to be bias corrected. The additional data from the soundings recorded during the 2006 AMMA (African Monsoon Multidisciplinary Analysis) campaign have been assimilated into the ARPEGE system, with and without a bias correction for relative humidity. Other assimilation experiments have used soundings which were received operationally at the time, or from a degraded pre-AMMA radiosonde network. The impact of different scenarii on the analysis and forecast over western Africa has been evaluated. For the full experiment using all data together with a bias correction, the humidity analysis and the daily and monthly averaged precipitation are improved. The impact of additional radiosonde observations is found to propagate downstream with a positive impact on forecast performance over Europe at the two and three-day forecast range (see Figure).

Whereas radiosonde observations have then shown to be very relevant, an important additional source of information is provided by satellite microwave data. These are more easily used over sea than over land and in-house developments have been necessary to advance the use of these data over the continents. Data assimilation experiments using for the first time ever AMSU-B humidity observations over land have emphasized strong drying and moistening features over Western Africa consistent with results obtained with the enhanced radiosonde network. The drying or moistening of the atmosphere have been successfully evaluated using independent humidity measurements. As a consequence, the African Monsoon appears to be better organized with a stronger Inter-Tropical Convergence Zone.
Both series of data assimilation experiments have shown that additional data over the African continent, either in situ or satellite-based, if carefully processed, can help to improve the description and prediction of the monsoon. The positive impact can also propagate in time during the forecast and affect Europe after a few days.

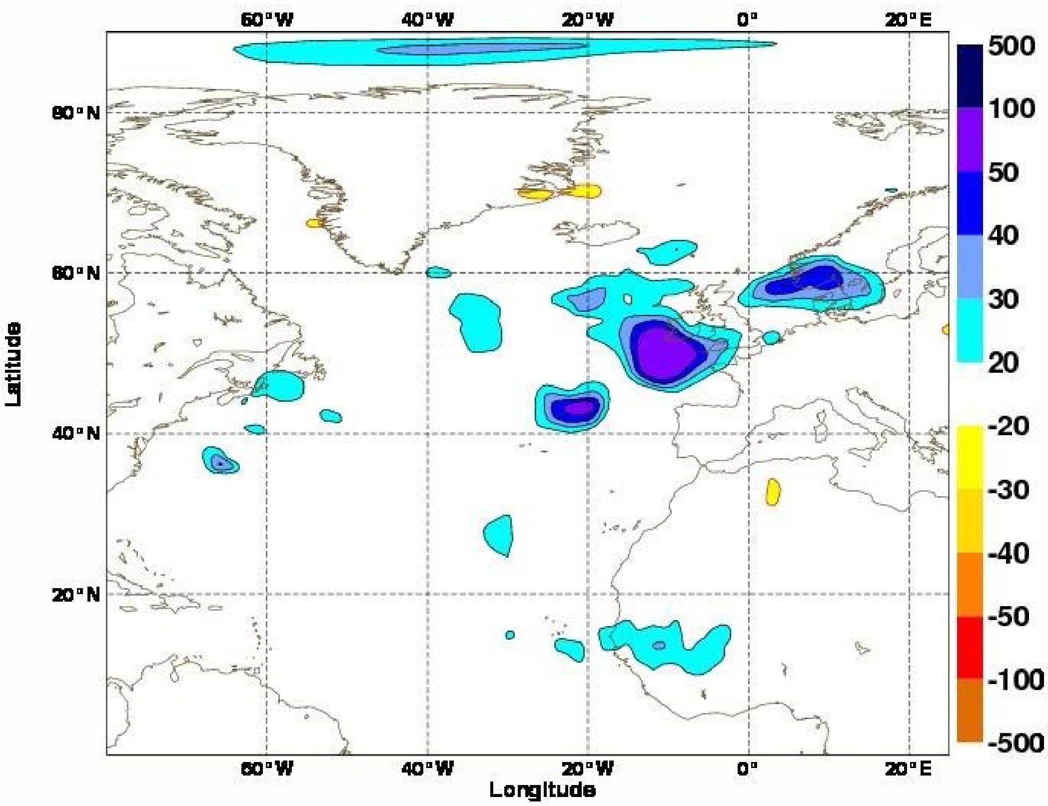

Figure caption: Differences in root-mean-square errors between the experiment using bias-corrected radiosonde AMMA data and the experiment using data from a network as in 2005. The errors are computed for the geopotential at 500 hPa at the 48h forecast range, over the period 1 August - 14 September 2006. Blue colours indicate that the AMMA data have contributed to improve the forecast.

An Update to the Quality Control Thresholds
of the Conventional Observing System for Global Data Assimilation

Masami SAKAMOTO
Numerical Prediction Division, Japan Meteorological Agency
1-3-4 Otemachi, Chiyoda-ku, Tokyo 100-8122, JAPAN
(e-mail: masami.sakamoto-a@met.kishou.go.jp)

The set of quality control (QC) thresholds used for global data assimilation by the Japan Meteorological Agency (JMA) was updated on November 10, 2008. This update improves the performance of operational global forecasting by the Global Spectral Model (GSM). Since the results of QC are also utilized for global/regional (Region-II) surface and upper-air observation monitoring by JMA, the thresholds were carefully modified so that the QC results for each observed quantity would be consistent with the previous results in their rejection rates.

1. An update to the QC thresholds used for JMA global data assimilation

A QC procedure named Dynamic-QC (Onogi, 1998) was adopted for the JMA global data assimilation system in March 1997. The temporal tendency and horizontal gradient of each physical quantity around an observation, which are estimated from a first guess (a short-term forecast), are used as predictors to determine QC thresholds. The procedure is applied to the quality control of geo-potential height, zonal and meridional wind speed, temperature, relative humidity and surface pressure reported by conventional observation contributors (SYNOP, SHIP, TEMP, AIREP and so on). Since this adoption, the same set of QC threshold coefficients had been used, while a number of developments in GSM and the global data assimilation system (including the Semi-Lagrangian dynamic scheme and 4D-Var) have been made.

In 2008, the QC thresholds were thoroughly reviewed to ascertain suitable levels for the current global NWP system. The dependencies of each threshold on the temporal tendency and horizontal gradient of each physical quantity were also re-evaluated. These dependencies were found to be quite different depending on latitude and height, and the thresholds for observed physical quantities are not necessarily dependent on such predictors. Figure 1 shows (a) the correlation coefficient and (b) the reliability of the Student's t-test of a linear regression between the QC threshold for temperature and the temporal tendency of temperature. It suggests that the temperature's QC threshold should be significantly dependent on its temporal tendency only below 100 hPa in the mid-latitudes of both hemispheres, but otherwise elsewhere. QC threshold coefficients (linear trends, interceptions and so on) for observed physical quantities without significant dependencies on the predictors were replaced with fixed QC thresholds.

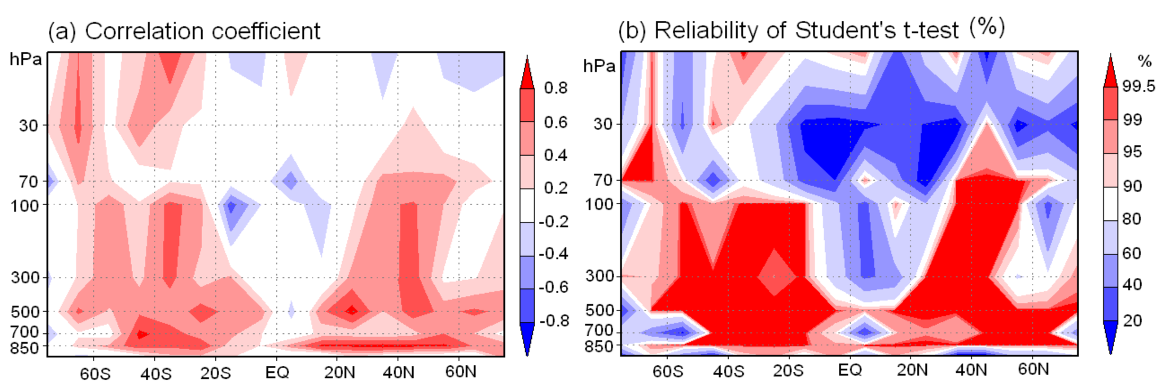

Figure 1. (a) Correlation coefficients and (b) reliabilities of the Student's t-test when a linear regression between the temperature's QC threshold and the temporal tendency of temperatures is performed. For the temperature's QC threshold, see Table 1.

An important application of the QC results is in observation data monitoring reports (see http://qc.kishou.go.jp/). These reports are utilized for observation quality improvements at each observation station. Accordingly, consistent QC results for each observed quantity are required.

Table 1 shows the QC (rejection) threshold and related statistical metrics obtained from global data assimilation experiments performed with the current GSM and assimilation system. As shown in the table, each threshold is defined using the average of absolute values of departures from the first guess (AAD) and the standard deviation of the departure (SDD). These statistics were updated, but since the definitions of the rejection thresholds remain unchanged, there is no significant change in the rejection rate for each observed quantity.

Table 1. Related statistical metrics and QC (rejection) thresholds. The metrics are obtained from an experiment performed from July 20 to September 9 of 2006. The metrics for each observed quantity are indicated using all observations regardless of the temporal tendency and horizontal gradient.

Observed Physical Quantity	Average of Absolute values of Departures from the first guess (AAD)			Standard Deviation of the Departures (SDD)			Rejection Threshold
	20°N – 90°N	20°S – 20°N	90°S – 20°S	20°N – 90°N	20°S – 20°N	90°S – 20°S	
500 hPa geo-potential height	17 gpm	18 gpm	12 gpm	150 gpm	124 gpm	51 gpm	AAD + 3 × SDD
850 hPa temperature	1.3 °C	1.4 °C	1.4 °C	1.9 °C	2.0 °C	2.0 °C	AAD + 3 × SDD
Surface pressure	0.8 hPa	0.9 hPa	0.8 hPa	1.7 hPa	2.8 hPa	2.8 hPa	AAD + 3 × SDD
300 hPa meridional wind speed	2.8 m/s	2.9 m/s	2.6 m/s	4.5 m/s	3.9 m/s	3.5 m/s	AAD + 3 × SDD
850 hPa zonal wind speed	2.4 m/s	1.9 m/s	1.9 m/s	3.4 m/s	2.7 m/s	2.5 m/s	AAD + 3 × SDD
700 hPa relative humidity	17.2%	20.7%	16.8%	24.6%	28.0%	22.8%	AAD + 4 × SDD

2. Improvement of forecast results

Figure 2 shows anomaly correlations of geo-potential height at 500 hPa over the Northern Hemisphere (20°N – 90°N) derived from preliminary forecast experiments performed for January and August 2007. Compared with the forecast results using the former QC thresholds, the new thresholds seem to contribute to an improvement in the forecast performance up to 192 hours (8 days). These results are believed to stem from the suitable QC thresholds for the current NWP system, which prevent erroneous observational reports from contaminating the initial fields of global forecasts.

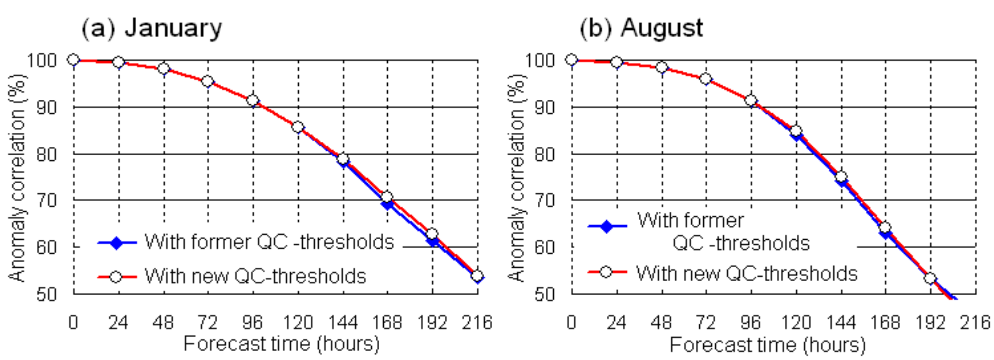

Figure 2. Anomaly correlations of geo-potential height at 500 hPa in the Northern Hemisphere (20°N – 90°N) against initial fields. The forecast results were examined for (a) January 2007 and (b) August 2007.

References

Onogi, K., 1998: A Data Quality Control Method Using Forecasted Horizontal Gradient and Tendency in a NWP System: Dynamic QC. *J. Meteor. Soc. Japan.*, 76, 497-516.

Synergistic effect of the assimilation of Radio occultation data and ground-based GPS data

Hiromu Seko, Kazuo Saito, Masaru Kunii,
and Yoshinori Shoji

Email: hseko@mri-jma.go.jp
Meteorological Research Institute, Tsukuba, Japan

1. Introduction

Radio waves transmitted from GPS satellite are delayed by atmosphere. Vertical profiles of refractivity and precipitable water vapor (PWV) are obtained from radio wave data received by low earth orbit satellites (LEO) and by GPS receivers on the ground. Because these data have the information of atmosphere, the assimilation methods for these data have been developed so far, and their impacts on heavy rainfalls or typhoon developments have been reported (e.g. Seko et al, 2004; Seko et al. 2009).

Seko et al. (2004) reported the impacts of GPS-derived water vapor data and radial wind of Doppler radar on the heavy rainfall. According to their results, PWV influenced the generation time of the rainfall region. When the slant water vapor (SWV) that is water vapor amount along the path from ground-based GPS receiver to GPS satellite were used, instead of PWV, water vapor distribution became more realistic one because slant water vapor data contains the information of vertical positions. As for vertical profiles of refractivity, they are estimated from the GPS radio occultation data (RO). Seko et al. (2009) reported the impact of RO data by using the method in which the path data from LEO to GPS satellite was assimilated in consideration of the vertical correlation of the observation error. They also showed that the intense rainfall was well reproduced by the assimilation of the occultation data.

Although the impacts of the RO data and PWV/SWV data were so far, synergistic effect has been not investigated. RO is high-resolution data in vertical direction. However, there is little information in the horizontal direction because the average of the path is assimilated (Fig. 1). On the other hand, SWV/PWV is high-resolution data in the horizontal direction. However, they have little information in the vertical direction. Thus, simultaneous assimilation of both data is expected to improve water vapor distribution because the information of both directions are used. In this study, we focus on the refractivity data of CHAMP (Challenging Mini-satellite Payload for Geoscientific Research and Application) and GPS-derived SWV to investigate the synergistic impact of these data.

2. Methodology

Figure 2 shows the rainfall amount from 12 JST to 15 JST 16 July 2004. On 16 July, intense rainfall band extending from west to east over the northern Japan developed. The methods used in this study are same as Seko et al (2004) and Seko et al (2009). The path between a GPS satellite and CHAMP passed south of this intense rainfall band. The lowest point of the path that was referred to as a tangent point reached the height of 2.8 km. When observed refractivity was compared with the first guess, the refractivity of the path data was larger below the height of 5 km (Fig. 3). The intensification of the rainfall is expected when RO data is assimilated. Figure 3 indicates the positions of ground-based GPS receivers. The GPS data of which receivers' heights exists within ±50 m were used to reduce the error caused by the assumption for the correction of height difference.

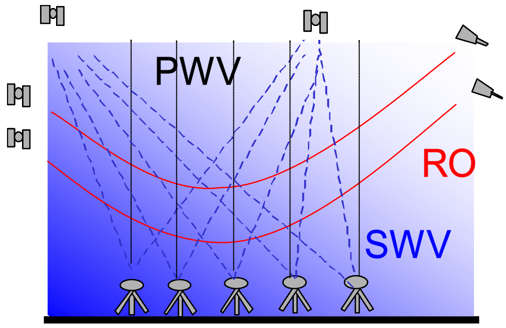

Fig.1 Schematic illustrations of assimilations of RO and SWV data.

3. Results of assimilation of RO and SWV data

Figure 5 indicates the results of the assimilation. When RO data was assimilated, the rainfall intensities over the northern Japan were intensified. However, the horizontal distribution extended more widely than observed one. When the SWV was assimilated, the rainfall region became similar to the observed one. However, the intensification remained weaker than the observed one. When RO and SWV were assimilated simultaneously, the shape and intensity were well reproduced. These improvements of the horizontal distribution and intensity of the rainfall band indicate that both data are needed to improve the horizontal distribution and intensity of the rainfall (the synergistic effect).

Next, the increments of the water vapor are explained. The assimilation of RO enhanced the contrast of the vertical distribution. Namely, water vapor of the lower layer near the rainfall band was more increased. The assimilation of SWV data intensified the horizontal contrast of the increment of the water vapor. The water vapor north of the rainfall region was decreased, while water vapor near the rainfall region was increased. This modified water vapor made the rainfall distribution similar to the observed one. When both data were assimilated, the contrast of increment was intensified in both directions.

Acknowledgements: CHAMP data and GPS data were provided from the GFZ and GSI. The authors would like to express the appreciation to GFZ and GSI.

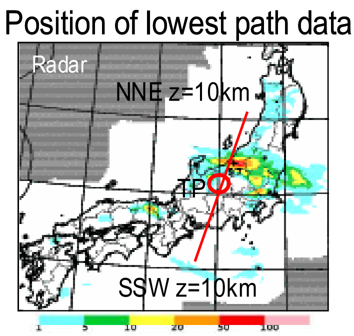

Fig. 2 Rainfall region at 15-18 JST 16 July observed operational radars. Red circle and line indicate the positions of a tangent points and the lowest path below 10 km.

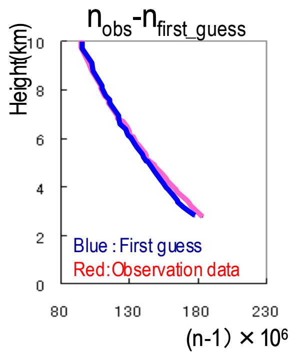

Fig. 3 Vertical profiles of observed refractivity at the tangent point and the corresponding first guess value.

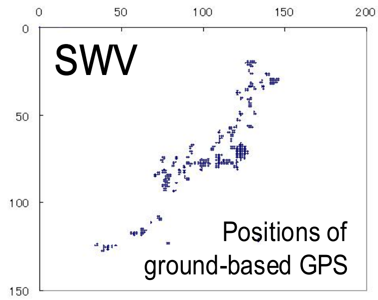

Fig. 4 Horizontal distribution of GPS receivers. GPS data of which receivers' heights exist within ±50 m are used in this study.

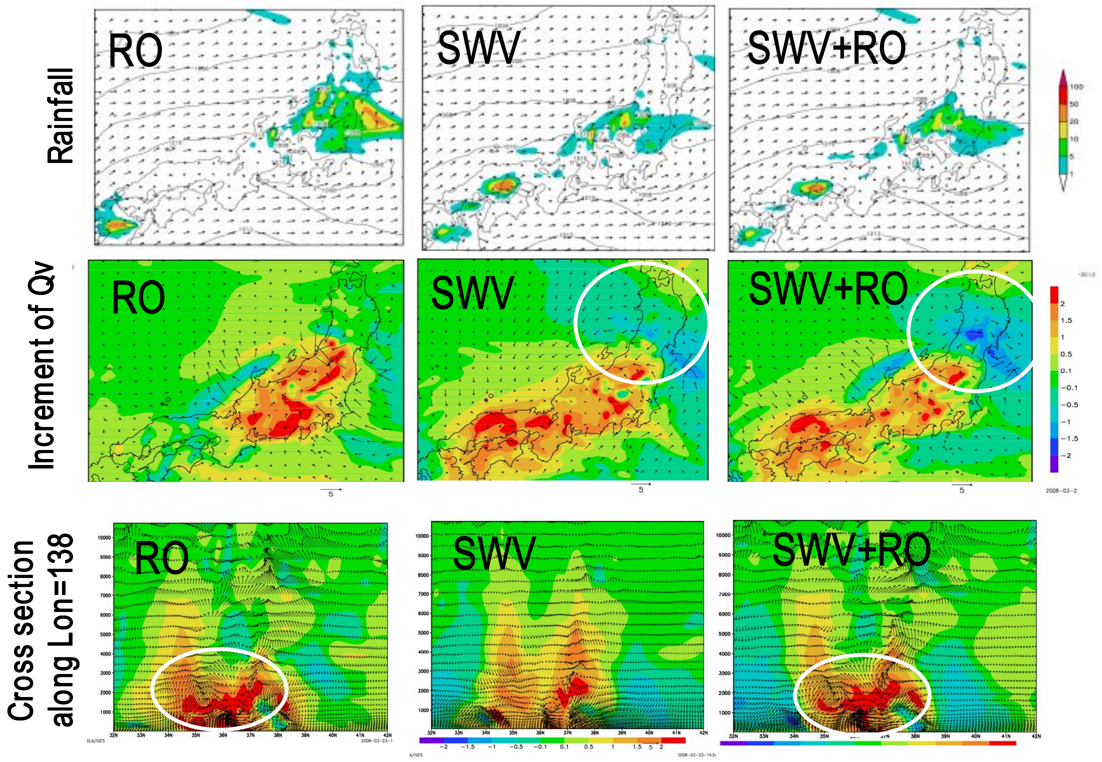

Fig. 5 (Upper panels): Rainfall distribution predicted from the initial fields obtained by assimilation of RO, SWV and both data. (Middle panels) Horizontal distributions of the increments of water vapor and horizontal wind at the lowest layer of the model. (Lower panel) Vertical cross sections of the increments of water vapor, northerly and vertical wind along the longitude of 138 degree.

Data assimilation experiment of the Kobe thunderstorm by using NHM-LETKF

Hiromu Seko[1], Kazuo Saito[1], Masaru Kunii[1],
and Takemasa Miyoshi[2]

Email: hseko@mri-jma.go.jp
[1] Meteorological Research Institute, Tsukuba, Japan
[2]Maryland University, Maryland, USA

1. Introduction

In ensemble Kalman filter (EnKF), data assimilation is performed with considering the error structure that fluctuates from day to day, and the initial perturbations of ensemble forecasts are produced by reflecting the analysis error properly. EnKF provides the probability of the occurrence of the significant phenomena. EnKF is expected to reduce the miss of the significant phenomena by using the forecast of ensemble members. In addition, the data assimilation of EnKF is easier than that of the variational method, because the adjoint model is not needed. Due to these merits, EnKF is expected to become one of useful techniques for mesoscale numerical prediction.

On 28 July 2008, the intense rainfall band was developed at Kobe Japan (Fig. 1), and 5 people in the river beach were claimed by the rapid rising of the Toga River. Unfortunately, this intense rainfall was not reproduced by the operational forecast model of JMA. In this study, the ensemble forecast was performed to reproduce this rain band by the assimilation of the GPS-derived precipitable water vapor (PWV). The object of this paper is to show the usefulness of the ensemble forecast and the impact of the PWV data on the forecast of heavy rainfall.

2. Methodology

In this study, a Local Ensemble Transform Kalman Filter (LETKF) (Miyoshi and Aranami, 2006) was used. The horizontal grid interval of LETKF was set to 20 km. This horizontal resolution was adopted to reproduce the mesoscale environment around the rainfall band within the limits of the computer resources. The domain of the experiments was 3300 km x 3000 km that covers the Japan main islands. Number of the ensemble member was 20. The cycle of the analysis and forecast was started at 72 hours before the occurrence of the intense rainfall band. The assimilation window period and assimilation slot interval were set to 6 hours and 1 hour, respectively.

As mentioned in the introduction, the intense rain band was not reproduced by the forecast of which initial condition was produced by the assimilation of the operational observation data. Thus, PWV data that were obtained from the GPS Earth Observation Network system of Geographical Survey Institute with the real time analysis methods (Shoji, 2009) was assimilated. Although the effect caused by the difference of the GPS receivers' heights and model topography was removed, the error produced by the assumption remained. To further reduce this error, the GPS-derived PWV, of which receivers' heights exist within ±50 m from those of the model topography heights of the GPS receivers' positions, was assimilated. To show the impact of the PWV data, two assimilation experiments were performed. In the first experiment, only operational observations, such as surface and upper sounding data, were assimilated. GPS-derived PWV was assimilated in addition to the operational data in the second experiment.

Non-hydrostatic model (NHM) of the Japan Meteorological Agency was used as the forecast model. Because the intense rainfall was composed of intense convections, downscale forecasts from the analyzed fields were also performed by NHM with the horizontal grid intervals of 5.0 km and 1.6 km.

3. Result of assimilation

Figure 2 shows the weather map at 09 JST (00 UTC) 28 July 2007. Baiu front extended north of the western Japan. The warm moist airflow (indicated by a thick arrow) moved around the western Japan, and then was supplied to the rainfall system of the front. At the 500 hPa, the cold air mass (indicated by a broken) was expanded to the Japan. Thus, the atmosphere over the western Japan had favorable condition for the generation and development of the thunderstorm.

Next, the observed PWV is compared with the first guess value (Fig .3). First guess value is the forecasted value from the former cycle's analysis fields. This comparison indicates that water vapor of the first guess was less humid than the observed ones at many GPS receivers over the Japan. Thus, rainfall is expected to be intensified by the assimilation of PWV.

Figure 4a shows the ensemble mean distribution of rainfall and surface pressure that was obtained by the assimilation of only the operational data. The synoptic scale features, such as a typhoon located near Taiwan, were reproduced. However, the rainfall was much weaker than the observed one. When this PWV data assimilated, the ensemble mean near Kobe was slightly expanded (Fig. 4b). This larger rainfall region indicates that PWV data has the positive impact for the forecast of the intense rainfall.

Next, the downscale experiments were performed with the grid interval of 5 km and 1.6 km. When the down scale experiments were performed, a few members reproduced the intense rainfall band (Fig. 5b). This result indicates that misses of severe events can be reduced by the performing the ensemble forecast. Because the environment (vertical profile of temperature etc.) around the rainfall band affects the rainfall amount, the relation between the rainfall amount and environments were plotted (Fig. 6). This scatter diagram shows that the temperature and equivalent potential temperature at the height of 500 hPa significantly influenced the rainfall amount. This result also indicates that ensemble forecasts provide the information of factors that cause the intense rainfall.

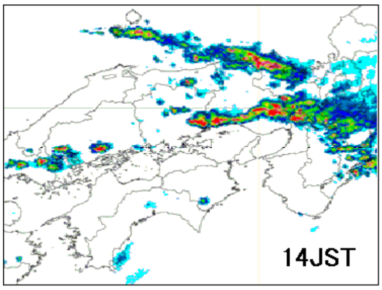

Fig. 1 Rainfall distribution observed by operational radar at 14 JST (05 UTC) 28 July 2008.

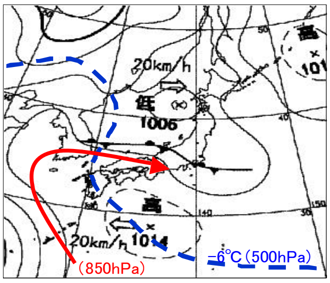

Fig. 2 Surface weather map at 09 JST (00 UTC) 28 July 2008.

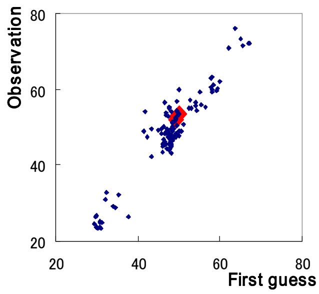

Fig. 3 Scatter diagram of the observed PWV and the first guess.

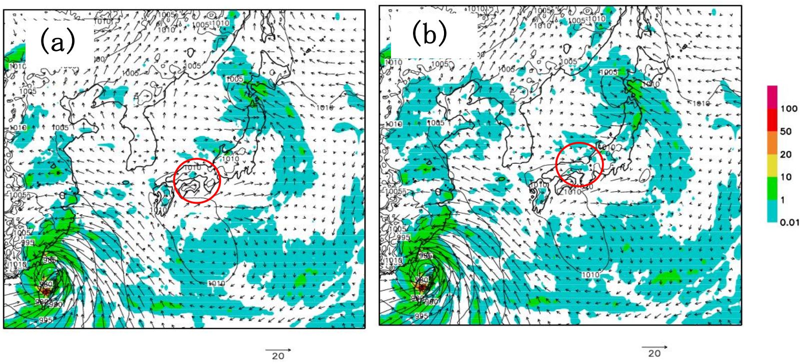

Fig. 4. Ensemble mean of rainfall and surface pressure at 15 JST (06 UTC) 28 July.

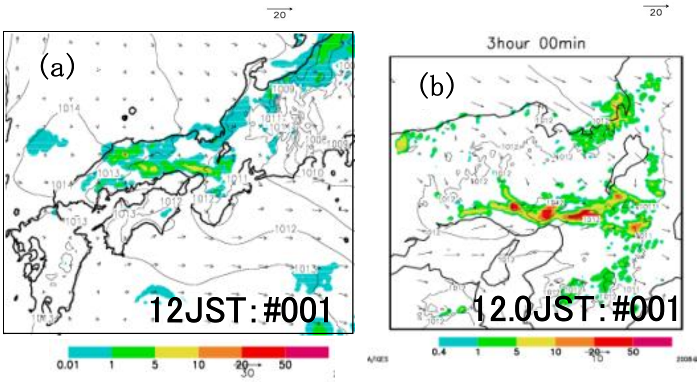

Fig. 5. Rainfall distribution at 12 JST (03UTC) reproduced by the downscale experiments using the NHM with the grind intervals of 5km and 1.6 km.

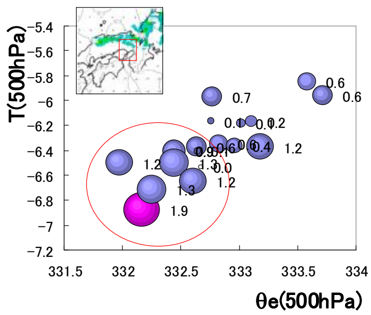

Fig. 6. Relations between average rainfall amount during 14-15 JST and the temperature or equitable potential temperature at 500 hPa in the read square region.

Local Ensemble Transform Kalman Filter for Semi-Lagrangian Barotropic Model of Atmosphere

A. Shlyaeva[1], *M. Tolstykh*[1,2]
e-mail: shlyaeva@gmail.com, tolstykh@inm.ras.ru
[1] Hydrometeorological Research Center of Russia, Moscow, Russia
[2] Institute of Numerical Mathematics, Russian Academy of Sciences, Moscow, Russia

Local ensemble transform Kalman filter (LETKF) data assimilation system is developed for global semi-Lagrangian barotropic model of atmosphere with external forcing.

The governing equation of the model is:

$$\frac{d\Omega}{dt} = F_{ext} \qquad (1),$$

where $\frac{d\Omega}{dt} = \frac{\partial\Omega}{\partial t} + \frac{u}{a\cos\varphi}\frac{\partial\Omega}{\partial\lambda} + \frac{v}{a}\frac{\partial\Omega}{\partial\varphi}$,

$\Omega = \Delta\psi + f + kH$, $\Delta\psi + f$ denotes vertical component of absolute vorticity, H stands for the orography, k is orography normalization coefficient, F_{ext} denotes external forcing, ψ – stream function, f – Coriolis parameter.

Equation (1) is discretized spatially like in [1]. The resolution of the model is $1.5^o \times 1.5^o$, time step is 45 minutes.

The external forcing F_{ext} is chosen so that the mean state of the system is close to the mean state of the actual atmosphere for the $\Delta\psi$ field at 300mb (averaged for the 5 days around the date of analysis) calculated from the NCEP/NCAR reanalysis.

Let $\Omega = \overline{\Omega} + \Omega'$, then

$$F_{ext} = \overline{\frac{u'}{a\cos\varphi}\frac{\partial\Omega'}{\partial\lambda} + \frac{v'}{a}\frac{\partial\Omega'}{\partial\varphi}} + \frac{\overline{u}}{a\cos\varphi}\frac{\partial\overline{\Omega}}{\partial\lambda} + \frac{\overline{v}}{a}\frac{\partial\overline{\Omega}}{\partial\varphi} - r\nabla^4\Omega + r\nabla^4\overline{\Omega}, \qquad (2)$$

where r is the diffusion coefficient.

The analysis of the properties for this system can be found in [2].

Local Ensemble Transform Kalman Filter [3, 4] is used for data assimilation. The only analysis variable is the vertical component of absolute vorticity. Pseudoobservations (the vertical component of absolute vorticity at 300mb calculated from the NCEP/NCAR reanalysis) are generated at random grid points and assimilated every 6 hours. The analysis ensemble consists of 40 members. The initial ensemble members of the background states are 40 ‘true’ fields (NCEP/NCAR reanalysis) of the vertical component of absolute vorticity at 300 mb, taken at the period from -20 to +19 dates from the first assimilation cycle date. All observations have equal weight within a 500 km radius of the grid point, beyond which the weight of the observations decreases exponentially with e-folding distance 800 km. Temporally varying adaptive covariance inflation algorithm [5] is applied.

Assimilation algorithm is parallelized via MPI for the number of processes equal to the number of ensemble members.

LETKF assimilation for the model (1) works stable for more than 4 months of assimilation. Time evolution of the L_2-norm for the analysis error with respect to the 'truth' (averaged over the randomly chosen observations) for the first 125 days (500 steps) of analysis is shown on Figure 1.

The goal of future research is to try different background covariance inflation algorithms (including spatially varying inflation), investigate the use of random perturbations and further investigate the properties of the system. It is planned to apply the implementation of the LETKF algorithm to a more sophisticated model.

Figure 1

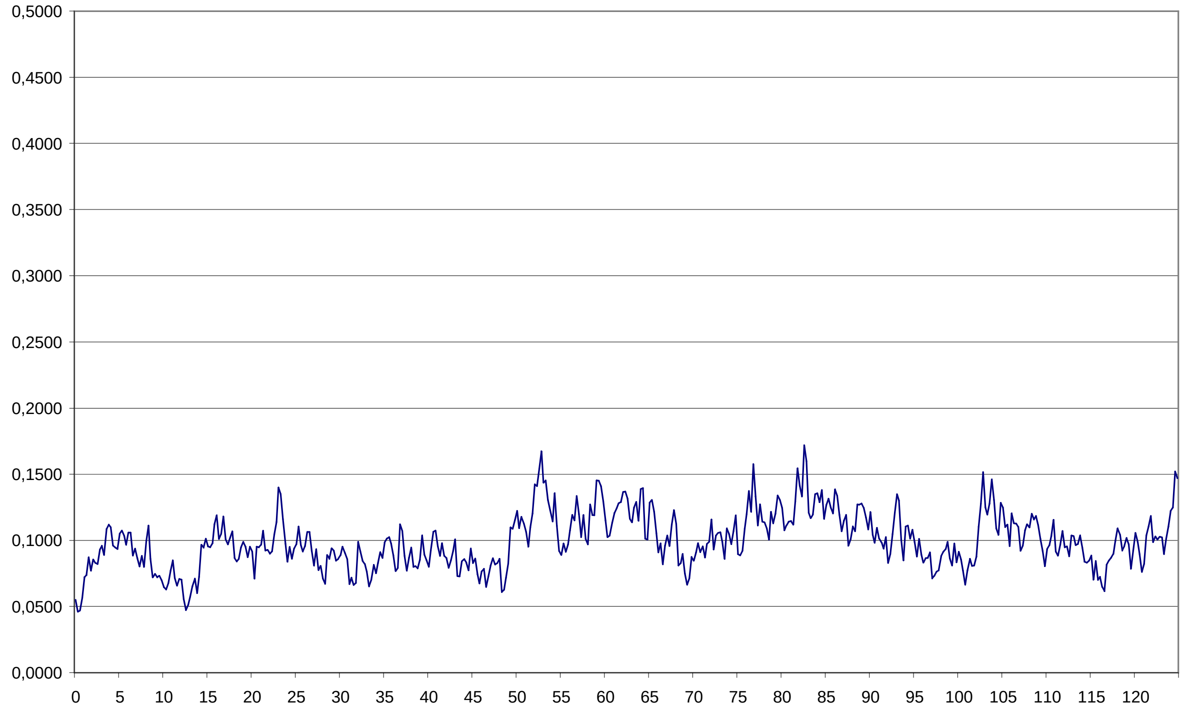

References

1. M.A. Tolstykh. Vorticity-divergence semi-Lagrangian shallow-water model on the sphere based on compact finite differences, J. Comput. Phys., 2002, v. 179, pp. 180-200.
2. A.S. Gritsun. Unstable periodic trajectories of a barotropic model of the atmosphere, Russ. J. Numer. Anal. Math. Modelling, 2008, v. 23, pp. 345-367.
3. Hunt, B.R., Kostelich, E.J. and Szunyogh, I. 2007. Efficient data assimilation for spatiotemporal chaos: a Local Ensemble Transform Kalman Filter. Physica D, 230, 112-126.
4. I. Szunyogh et.al. A local ensemble transform Kalman filter data assimilation system for the NCEP global model, Tellus, 2008, v. 60, pp. 113-130.
5. Hong Li, E. Kalnay, T. Miyoshi. Simultaneous estimation of covariance inflation and observation errors within an ensemble Kalman filter, submitted to QJRMS.

Assimilation of radar data at convective scale at Météo-France

By Eric Wattrelot and Thibaut Montmerle

CNRM/GAME, Météo-France and CNRS
42 av Coriolis
31057 Toulouse
France
eric.wattrelot@meteo.fr

These last years, Météo-France has developed a Numerical Weather Prediction (NWP) system at convective scale that has been running operationally since the 18th December 2008. This system, called AROME, covers the French territory with a 2.5 km horizontal resolution. Its main goals are to improve the local meteorological forecasts of potentially dangerous convective events (storms, unexpected floods, wind bursts, etc.) and of lower tropospheric phenomena (wind, temperature, turbulence, visibility, etc.). AROME uses the physical parameterisations from the non-hydrostatic MesoNH model that considers in particular complete representation of the water cycle with five hydrometeors governed by a bulk microphysical parameterisation. AROME makes use of a complete data assimilation system derived from the ALADIN 3Dvar that is operationally running at Météo-France at regional scale since the end of 2005. In this context, radial velocities and volumes of reflectivities observed by the national ARAMIS Doppler radar network play a key role by providing information about the horizontal wind circulation and the 3D precipitation patterns within precipitating systems over a wide part of France with high horizontal and temporal resolutions.

To assimilate such quantities, observation operators, that allow to simulate the radar measurements at the observed locations, have been developed. The assimilation of Doppler winds in the AROME 3Dvar has been validated on several convective cases and evaluated on a daily basis in a pre-operational configuration. It has been shown that, when some favourable sampling conditions are present, short term forecasts of precipitations are improved thanks to a more realistic analysis of convergence structures in the boundary layer (Montmerle and Faccani, 2009). Following these results , Doppler winds of 16 radars have been included in the first operational AROME NWP system.

An important evolution will be the assimilation of radar reflectivities, which is routinely evaluated since the end of 2008. As it is stated in Caumont *et. al* (2006), the direct observation operator of reflectivities requires complete warm and cold microphysical parameterization which consider nonlinear moist processes and thresholds (convection regimes and saturation in particular). To avoid problems in the minimization algorithm, an original “1D+3DVar method” to assimilate these radar reflectivities has been introduced. The 1D algorithm consists of a Bayesian statistic method which allows to retrieve relative humidity profiles from the observed columns of reflectivities, the different hydrometeor types being not analysed. For this, the model state in the vicinity of the observation is used as source of information, in order to assess the necessary information about precipitating species to constraint the solution. The method must provide the most probable profile by application of Bayses’ theorem. The retrieved humidity profiles are then directly assimilated in the 3Dvar. The method has proved the capability to create proper increments to adjust the model reflectivities towards the observations, even if there is no rain (at the same location) in the model background fields (Wattrelot *et al,* 2008). In order to dry and shift misplaced precipitating patterns, it has been shown that the assimilation of the “no-rain” signal provided by the radars was very useful (see figure). An evaluation of two months of cycled assimilations has confirmed a good impact on scores of precipitating forecasts.

A recent work with the producers has led to a better characterization of the "no-rain" signal which depends of the sensitivity of each radar, which is a decreasing function with the range from the radar. Sensitivities studies on analysis of this detection threshold have allowed to define the best careful using of the "no-rain" signal.

In the short term, a similar work to better characterize clutter (in particular clear sky echoes and see clutter) will allow to use Doppler winds of additional radars (including coastal) operationally. Assimilation of reflectivities still is evaluated on a daily basis, and should hopefully be included in the operational suite at the end of 2009.

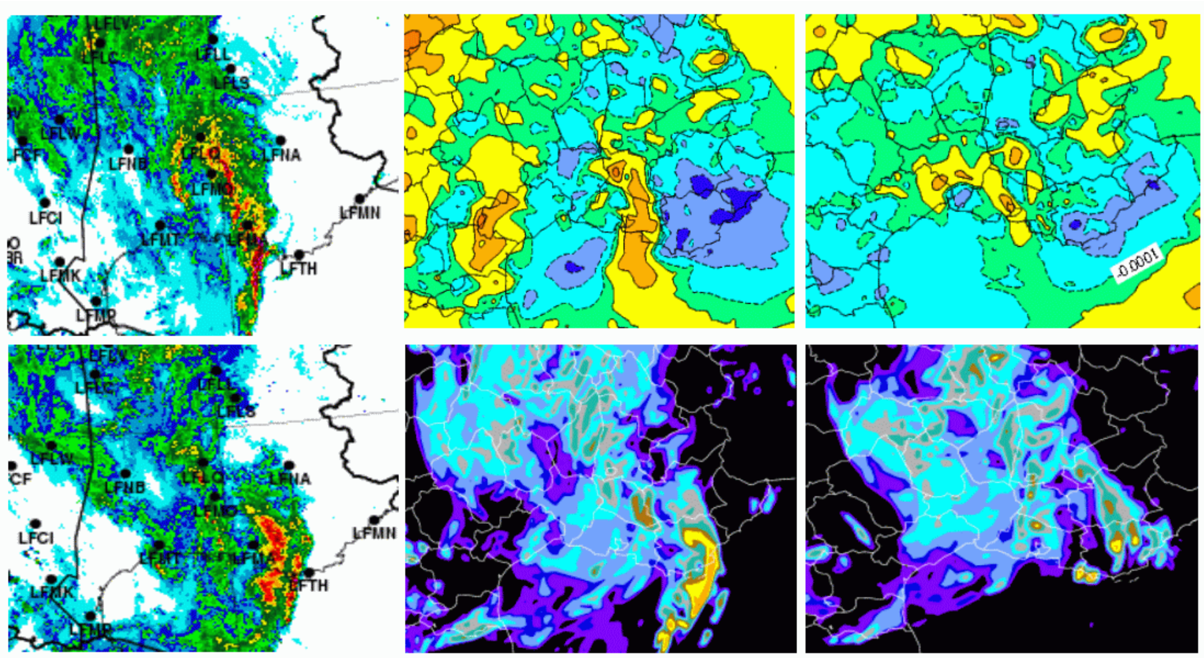

Figure caption: Squall line on the South-East of France the 8th October 2008. Top panels: at 06h UTC, composite reflectivity pattern (left), analysis increments of specific humidity at 850 hpa deduced from the AROME assimilation system with (middle) and without (right) radar reflectivities (yellow-orange contours denote positive increments, isocontours every 0,1 g/kg). Bottom panels: at 09h UTC, composite reflectivity pattern (left), 3h AROME forecast of the 900 hpa simulated reflectivity field from an analysis provided by the assimilation cycle with (middle) and without (right) reflectivities.

Caumont O., Ducrocq V., Delrieu G., Gosset M., Parent du Châtelet J., Pinty J.-P., Andrieu H., Lemaître Y., Scialom G., 2006. A Radar Simulator for High-Resolution Nonhydrostatic Models. *J. Atmos. Oceanic. Technol.*, **23**: 1049–1067

Montmerle, T and C. Faccani, 2008: Mesoscale assimilation of radial velocities from Doppler radar in a pre-operational framework. *Mon. Wea. Rev*, in press.

Wattrelot E, Caumont O., Pradier-Vabre S., Jurasek M. and Günther Haase , 1D+3DVar assimilation of radar reflectivities in the pre-operational AROME model at Météo-France. ERAD2008. *Proceedings of the fifth European conference on radar in meteorology and hydrology.*

An Observing System Experiment on the Special Observations of T-PARC for Typhoons Sinlaku and Jangmi using the Operational NWP System at JMA

Koji Yamashita*, Yoichiro Ohta* and Tetsuo Nakazawa**
*Numerical Prediction Division, Japan Meteorological Agency
**Meteorological Research Institute, Tsukuba, Japan
E-mail: kobo.yamashita@met.kishou.go.jp

1. Introduction

A special observation experiment project that examined the effectiveness of the next-generation forecast technology known as the *interactive forecast system* was performed as part of the THORPEX Pacific Asian Regional Campaign (T-PARC) for track forecasts of three typhoons (Nuri, Sinlaku and Jangmi) in the summer of 2008 at JMA (T-PARC 2008). The special observations performed for T-PARC 2008 were dropwindsonde observations, extra radiosonde observations at JMA observatories and ships observations (Komori et al., 2009). JMA's Meteorological Satellite Center also produced MTSAT-2 Rapid Scan Atmospheric Motion Vectors for T-PARC 2008. As one of the research projects, typhoon-track and intensity forecast experiments for Sinlaku and Jangmi were performed using special observational data in the operational NWP system at JMA.

2. Overview of the experiments

To evaluate the impact of the special T-PARC 2008 observations, we carried out experiments using the operational global 4D-Var data assimilation system (GSM-DA). Global 4D-Var data assimilation cycles were run every 6 hours, and 84-hour forecasts were executed from 00, 06 and 18 UTC and 216-hour forecasts from 12 UTC using the operational global spectral model (JMAGSM). The JMAGSM is a hydrostatic spectral model with a horizontal resolution of 20 km (the inner-loop model for the GSM-DA is 80 km) and 60 levels in the vertical direction, with the top level at 0.1 hPa.

The two typhoons were spawned in September 2008. The experimental periods were from 00 UTC on 9 September (0900; hereafter the date and time are abbreviated as *ddhh* without the month) to 1818 for Sinlaku and from 2500 to 2818 for Jangmi. We performed two kinds of numerical experiments that differed in their use of special observations: (I) special observations were assimilated (TEST), and (II) special observations were not assimilated (CNTL).

JMA assimilates bogus data to generate realistic typhoon structures in the analysis fields of the operational system (JMA, 2007). Bogus data were not used in the observing system experiment (OSE) for Sinlaku, but were assimilated in the OSE for Jangmi.

3. Impact of special observations on typhoon-track and intensity predictions

The typhoon-track forecasts from the OSEs were verified against the best track data analyzed by JMA (OBS). Since the special observations were concentrated both in the before-recurvature stage and the after-recurvature stage, the results were separately validated for each.

In many cases, positive impacts were found on typhoon-track and intensity forecasts using the special observations in each stage. These results suggest that the special observations contributed to reducing track and intensity errors. The details for each typhoon are outlined below.

A. Sinlaku

In the before-recurvature stage from 0900 to 1418, the track errors of TEST were reduced by between 23 and 30% for 12-hour forecasts, and by approximately 10% for 18- to 48-hour forecasts compared to the results of TEST for CNTL (Fig. 1). A forecast initialized at 0912 is shown in Fig. 2. Intensity forecast errors were also reduced in this case. In the after-recurvature stage, the track errors of TEST were reduced by about 10% for 66- to 84-hour forecasts. However, the impact on the intensity forecasts was neutral.

B. Jangmi

In the before-recurvature stage from 2500 to 2818, the track errors of TEST were reduced for forecasts of up to 84 hours (Fig. 3). The mean reduction rate of track errors was 25%. The maximum reduction rate was 36% for 12-hour forecasts. A forecast initialized at 2500 is shown in Fig. 4. In the after-recurvature stage from 2900 to 3018, the track errors of TEST were reduced by between 12 and 20% for 18-hour forecasts.

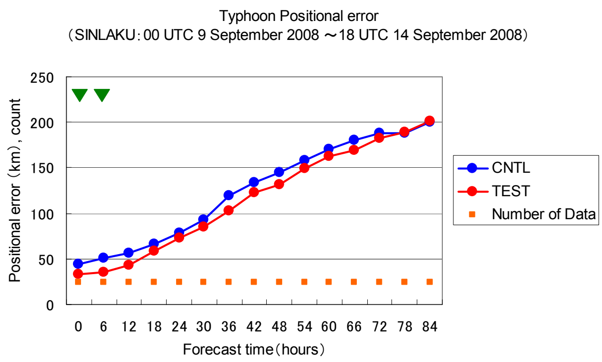

Figure 1. Positional errors for Typhoon Sinlaku in the before-recurvature stage from 0900 to 1418. The red line with dots is for TEST, which assimilated special observations. The blue line with dots is for CNTL, which did not assimilate special observations. The orange squares indicate the number of cases, and the green triangles denote that the difference is statistically significant with a 95% confidence level.

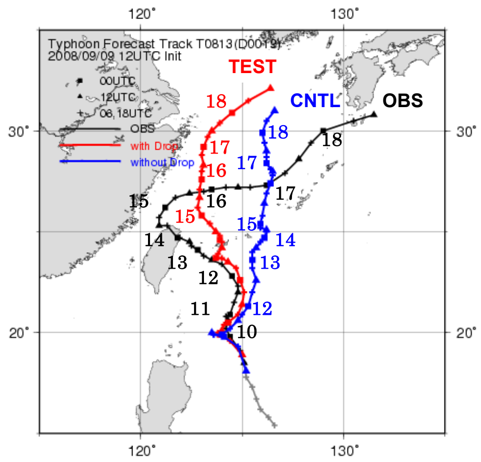

Figure 2. Typhoon track forecasts by OSEs with (red markers: TEST) and without (blue markers: CNTL) special observations for Typhoon Sinlaku, initialized at 0912. The numbers indicate the date of the typhoon's location at 00 UTC.

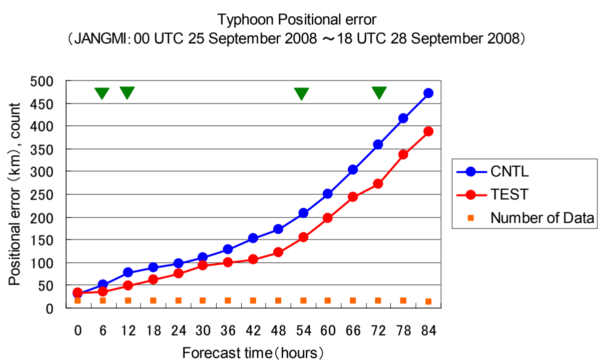

Figure 3. Positional errors for Typhoon Jangmi in the before-recurvature stage. The legend details are the same as those in Fig. 1, but the period is from 2500 to 2818.

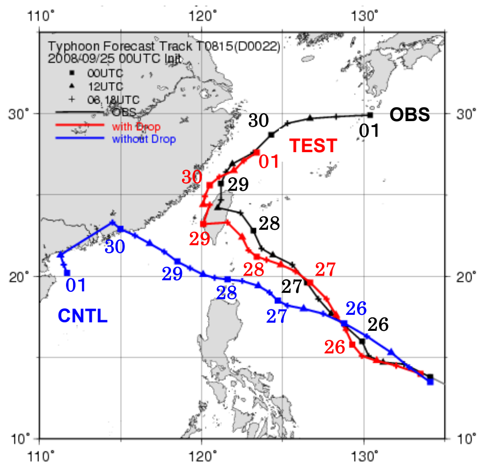

Figure 4. Typhoon track forecasts by OSEs with (red markers: TEST) and without (blue markers: CNTL) special observations for Typhoon Jangmi, initialized at 2500

REFERENCES

JMA 2007: OUTLINE OF THE OPERATIONAL NUMERICAL WEATHER PREDICTION AT THE JAPAN METEOROLOGICAL AGENCY March 2007, 17

Komori, T., R. Sakai, H. Yonehara, K. Sato, T. Miyoshi, M. Yamaguchi and T. Nakazawa, 2009: JMA's Total Energy Singular Vector Sensitivity Guidance for Adaptive Observations during T-PARC 2008.CAS/JSC WGNE Research Activities in Atmospheric and Oceanic Modeling, 41, submitted.

WMO 2008: THORPEX PROGRESS REPORT March 2008, 1-17 [Available from http://www.wmo.int/pages/prog/arep/wwrp/new/documents/THORPEX_report_March_2008.pdf]